

Estimation of mass outflow rates from viscous relativistic accretion discs around black holes

Indranil Chattopadhyay¹, Rajiv Kumar^{1*}

¹*Aryabhata Research Institute of Observational Sciences (ARIES), Manora Peak, Nainital-263002, India*

ABSTRACT

We investigated flow in Schwarzschild metric, around a non-rotating black hole and obtained self-consistent accretion - ejection solution in full general relativity. We covered the whole of parameter space in the advective regime to obtain shocked, as well as, shock-free accretion solution. We computed the jet streamline using von - Zeipel surfaces and projected the jet equations of motion on to the streamline and solved them simultaneously with the accretion disc equations of motion. We found that steady shock cannot exist for $\alpha \gtrsim 0.06$ in the general relativistic prescription, but is lower if mass - loss is considered too. We showed that for fixed outer boundary, the shock moves closer to the horizon with increasing viscosity parameter. The mass outflow rate increases as the shock moves closer to the black hole, but eventually decreases, maximizing at some intermediate value of shock location. The jet terminal speed increases with stronger shocks, quantitatively speaking, the terminal speed of jets $v_{j\infty} > 0.1$ if $r_{\text{sh}} < 20r_{\text{g}}$. The maximum of the outflow rate obtained in the general relativistic regime is less than 6% of the mass accretion rate.

Key words: accretion, accretion disc - black hole physics - Hydrodynamics - shock waves.

* E-mail: indra@aries.res.in (IC); rajiv.k@aries.res.in (RK)

1 INTRODUCTION

Large amount of radiation emitted by astrophysical objects like microquasars and active galactic nuclei (AGNs) favours the scenario that such energy output is due to the conversion of gravitational energy of matter into heat and radiation as it falls into extremely relativistic objects like black holes (BHs). Microquasars are essentially X-ray binaries and are supposed to harbour a stellar mass BH ($M_{\text{BH}} \sim 10M_{\odot}$), while AGNs harbour supermassive BH i.e. $M_{\text{BH}} \sim 10^6\text{--}10^9M_{\odot}$. The radiation emitted by these objects in general contains a relatively low energy multi-coloured blackbody component and one or more power-law components in the higher energy limit. When the accretion disc is in a state, from which the power emitted maximizes in the higher energy region and the luminosity is low, it is called the low/hard (LH) state. When the power maximizes in the lower energy level, the disc is luminous and produces multi-coloured blackbody radiation, it is called the high/soft state (HS). There are many intermediate states (IM) which connects the two. Along with energetic photons, AGNs and microquasars also eject highly energetic, collimated and relativistic bipolar jets. Observations of a large number of microquasars showed that the jets are seen only when the accretion is in the LH or IM, but the jet is not seen when the accretion disc is in canonical HS spectral state (Gallo et. al. 2003; Fender et. al. 2004; Fender & Gallo 2014), i.e. the jet states are correlated with the spectral states of the accretion disc. Such a correlation between spectral states and jet states cannot be made in AGNs, partly, because of the longer timescale associated with supermassive BHs and partly, due to possible lack of the periodic repetitions of the outer boundary condition of AGN accretion discs. However, the fact that timescales in AGNs and microquasars can be scaled by mass (McHardy et. al. 2006) tells us that the essential physics around super-massive and stellar mass BHs are similar.

The first popular model of accretion disc around BH was proposed by Shakura & Sunyaev (1973) and Novikov & Thorne (1973), and is known as Keplerian disc or standard disc or Sakura-Sunyaev (SS) disc. It is characterized by matter rotating with local Keplerian angular velocity, with negligible infall velocity, and is geometrically thin but optically thick. Being optically thick, each annuli emits radiation which is thermalized with the matter. Each annulus has different temperature and therefore the spectrum emitted is a sum of all the blackbody radiations from each of the annuli, i.e. multi-coloured blackbody spectrum. Indeed, the thermal radiation part of a BH candidate spectrum is well explained by a Keplerian disc. Although SS disc was very successful in explaining the thermal component of the spectrum

emitted by BH candidates, but it could not explain the hard powerlaw tail. The inner boundary condition of the SS disc is quite arbitrary and is chopped off within the marginally stable orbit. The pressure gradient term and the advection term in SS disc are also poorly treated. It was realized that there should at least be another component in the disc, which would behave like a Comptonizing cloud of hot electrons to produce the hard power-law tail (Sunyaev & Titarchuk 1980). Moreover, the inner boundary condition of BH dictates that matter crosses its horizon with the speed of light, and that the angular momentum of the flow close to the horizon needs to be necessarily sub-Keplerian. Therefore, in addition to SS discs, investigations of accretion in sub-Keplerian regime also gained prominence, such as thick accretion discs (Paczynski & Wiita 1980), advection-dominated accretion flows or ADAF (Narayan *et al.* 1997), advective-transonic regime (Liang & Thompson 1980; Fukue 1987; Chakrabarti 1989). All these models start with exactly the same set of equations of motion i.e., Navier-Stokes equation in strong gravity, but differ in boundary conditions. For example, if the radial advection term and the pressure gradient term are negligible, azimuthal shear is responsible for viscosity and the heat dissipated due to viscosity is thermalized locally and efficiently radiated out, then the resulting disc is the SS disc. On the other hand, if only the advection term is negligible and the cooling is less efficient, then the model is thick disc. The ADAF and the transonic regime are not subjected to such confinement, in fact, Lu *et al.* (1999) showed that global ADAF is indeed a subset of general transonic solutions. Recently, by playing around with the viscosity parameter and cooling efficiency in the computational domain, Giri & Chakrabarti (2013) were able to generate both sub-Keplerian advective disc and Keplerian disc simultaneously. The Keplerian disc gives out soft photons, and sub-Keplerian flow supplies hot electrons, if the disc has a shock transition. The post-shock disc behaves like a Comptonizing cloud, and produces the hard power-law photons.

The transonic/advective disc has several advantages. It satisfies the inner boundary condition of the BH, i. e., matter crosses the horizon at the speed of light and therefore it is supersonic and sub-Keplerian. It implies that the existence of a single sonic point (the position where bulk velocity crosses the local sound speed) is guaranteed around a BH. However, depending on the angular momentum, there can be multiple sonic points. As a consequence, matter accelerated through the outer sonic point can be slowed down due to the presence of centrifugal barrier. This slowed down matter may impede the supersonic matter following it, and may cause shock transition (Fukue 1987; Chakrabarti 1989). Shock in BH accretion has been found to exist for inviscid flow (Fukue 1987; Chakrabarti 1989;

Aktar et al. 2015), dissipative flow (Das 2007; Kumar & Chattopadhyay 2013), and has also been confirmed in simulations (Molteni *et al.* 1996b; Lee *et al.* 2011; Das *et al.* 2014). The post-shock region of the disc (PSD), has some special properties. Apart from producing hard powerlaw photons, it was shown for an inviscid disc via numerical simulations, that the extra thermal gradient force in the PSD powers bipolar jets (Molteni *et al.* 1994, 1996a), and was later established for viscous disc as well (Lanzafame *et al.* 1998; Chattopadhyay & Das 2007; Das & Chattopadhyay 2008; Kumar & Chattopadhyay 2013; Das *et al.* 2014; Kumar *et al.* 2014). Moreover, since the jet originates from PSD (which extends from few to few tens of Schwarzschild radii) and not the entire disc, it satisfies the observational criteria that jets are generated from the inner part of the accretion disc (Junor et. al. 1999; Doeleman et. al. 2012).

Most of the theoretical studies of accretion on to BHs have been in the domain of pseudo-Newtonian potential (pNp) (Paczyński & Wiita 1980) and fixed adiabatic index (Γ) equation of state (EoS) of the flow. Using pNp gravity potential instead of the Newtonian one has the advantage that, the Keplerian angular momentum distribution, the location of marginally stable orbit (r_m), marginally bound orbit (r_b), or, the photon orbit (r_{ph}) can be obtained exactly, as is obtained in general relativity (GR), but can still remain in the Newtonian regime of physics. However, according to relativity, matter cannot achieve the speed of light (c) outside the horizon, but, in pNp regime matter velocity exceed c outside the horizon. The effective potential of a rotating particle is zero on the horizon in GR, however, it is negative infinity on the horizon if we use pNp. Moreover, in relativity the physics of fluid is different from that of the particles. This arises because in relativistic equations of motions the thermal term, the angular momentum term etc, couples with the gravity. As a result, for conservative systems, the constants of motion are not the same in particles and fluids. While in pNp regime, the constants of motion in fluid and particles are identical. For viscous flow, the shear tensor in relativity is much more complicated and contains many more terms when compared to the shear tensor in pNp regime. Therefore, solutions of relativistic equations for transonic accretion discs around BH have been few (for e.g. Liang & Thompson 1980; Lu 1985; Fukue 1987; Chakrabarti 1996) when compared with those in pNp regime and that too in the inviscid limit. The first consistent viscous advective accretion solution in pure GR was obtained by Peitz & Appl (1997). They derived the shear tensor from the first principle, and then approximated it with a simpler but accurate function. For inviscid flow the constants of motions are the relativistic Bernoulli parameter ($\mathcal{E} = -hu_t$, h is the enthalpy and u_t is the

covariant time component of the four velocity), the accretion rate, angular momentum and the entropy along a streamline. For viscous flow, except the accretion rate, none of these are constant along the motion, and constants of motion need to be determined. The information of the constants of motion were not used at all by Peitz & Appl (1997), which resulted in a limited class of solutions. Moreover, they did not discuss the issue of mass loss either. We would like to rectify that, i. e., to say we would like to obtain all possible accretion solutions using constants of motion and constants of integration, as well as, estimate the mass loss from the accretion solution.

Another limitation of a large body of work on accretion-ejection solutions around compact objects is that, most of the work has been done assuming a fixed Γ equation of state (EoS), where, Γ is the adiabatic index. From classical fluid mechanics, we know that Γ is the ratio of specific heats, which turns out to be equal to the constant $5/3$, if random motions of the constituent particles of the gas are negligible compared to c . However, if the random speeds of the particles is comparable to c , then Γ is not constant and the EoS becomes a combination of modified Bessel's function of the inverse of temperature (Chandrasekhar 1939; Synge 1957; Cox & Giuli 1968). It can be trivially shown that the different forms of the exact EoS obtained by the above three authors are equivalent (Vyas et al. 2015). Moreover, it has been shown that it is unphysical to use fixed Γ EoS when the temperature changes by a few orders of magnitude (Taub 1948). The first accretion solution using a relativistic EoS on to a Schwarzschild BH was obtained by Blumenthal & Mathews (1976). Takahashi (2007) regenerated the solutions of Peitz and Appl, but also obtained solutions with another form of viscosity using variable Γ EoS in Kerr-Schild metric. However, the EoS used was again for a fluid composed of similar particles. Fluids around BH should be fully ionized given the temperature associated with these fluids, and ionized single species fluid can only be electron-positron flow which cannot exist for thousands of Schwarzschild radii around the BH. Blumenthal & Mathews (1976) however, hinted how to describe a fluid composed of different particles. Fukue (1987) in a seminal paper solved accretion solutions in the advective domain for electron-proton flow, and predicted the possibility of accretion shocks around BH. The inherent problem of using the exact relativistic EoS in simulation codes is that, it is a ratio of modified Bessels function which make transformation between primitive variables and state variables non-trivial. To circumvent this problem we obtained an approximate EoS which is very accurate (Ryu *et al.* 2006) for single species fluid, and then extended it to multi-species fluid (Chattopadhyay 2008; Chattopadhyay & Ryu 2009;

Chattopadhyay & Chakrabarti 2011). The adiabatic EoS was also obtained for such a flow by integrating the entropy generation equation without source terms (Kumar *et al.* 2013). The comparison of Chattopadhyay-Ryu (CR) EoS with an exact one showed negligible difference between the two (Vyas *et al.* 2015). The approximate CR EoS was also used in the pNp regime to study dissipative accretion flow (Kumar & Chattopadhyay 2014), which showed that accretion shocks may exist for very high viscosity, as well as, high accretion rates. Moreover, depending on these flow parameters such discs can be of low luminosity, as well as, can emit above the Eddington limit. Interesting as it may be, but we know pNp regime can only be considered to be qualitatively correct, and a general relativistic viscous disc should be considered to fully understand the behaviour of such discs. Investigations of general relativistic, dissipative, advective accretion discs around BH, described by relativistic EoS has not been done for multi-species EoS, in addition, estimation of mass loss from such disc has not been undertaken as well. Apart from the highly non-linear equations of motion in GR to contend with, it is also a fact that in curved space time, the constant angular momentum surfaces are special surfaces called von-Zeipel surfaces (e. g. Chakrabarti 1985, and references therein). Jets launched with some angular momentum would follow these surfaces. So an accretion-ejection system in GR is significantly different from pursuing the same study in pNp regime. In this paper, we obtain a simultaneous, self-consistent bipolar jet solution from a general relativistic viscous disc around a BH, described by multi-species relativistic EoS.

In the next section, we present the equations of motion for the accretion disc and the jet, and also a brief description of the EoS used. In Section 3, we present the solution procedure of the equations of motions. In Section 4, we present the results, and then present our concluding remarks in Section 5.

2 ASSUMPTIONS AND EQUATIONS

In this section, we first present the equations of motion governing the accretion disc and then those governing the matter leaving the disc as bipolar jets. Although equations of motion for both disc and jets are conservation of four-momentum and four-mass flux, but since the flow geometry of the disc and that of the jet are different, we will separately present the two sets of equations. In Fig. 1, a cartoon diagram of the disc jet system is presented. The accretion disc occupies the region around the equatorial plane, while the jet flows about the

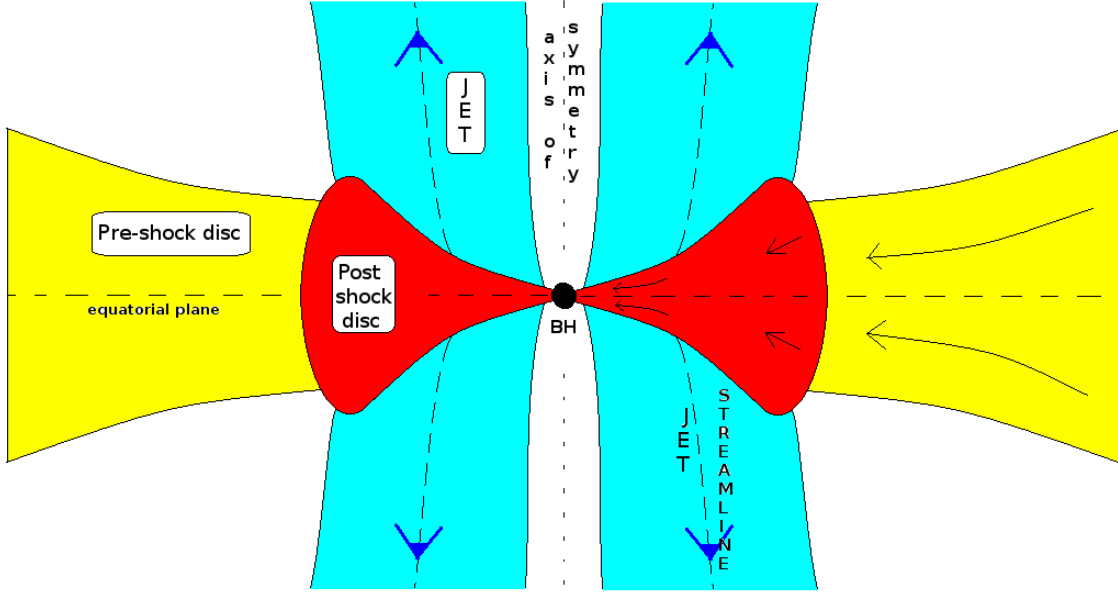


Figure 1. Cartoon diagram of disc-jet system. The arrows show the direction of motion. The disc flow geometry is on and around the equatorial plane, while the jet flow geometry is about the axis of symmetry. The post-shock disc or PSD and the pre-shock disc are shown. The jet streamline is also mentioned. Here BH stands for the black hole.

axis of symmetry. The jet geometry is significantly different from the pNp prescription and will be described in Section 2.3.

2.1 Equations governing accretion disc

The energy momentum tensor for the viscous flow is

$$T^{\mu\nu} = (e + p)u^\mu u^\nu + pg^{\mu\nu} + t^{\mu\nu}, \quad (1)$$

where e , p and u^μ are the local energy density, local gas pressure and four-velocities, respectively. The inverse of the metric tensor components is $g^{\mu\nu}$ and Greek indices μ, ν represent the space-time coordinates. Here, $t^{\mu\nu}$ is viscous stress tensor and considering it is only the shear that gives rise to the viscosity, then $t^{\mu\nu} = -2\eta\sigma^{\mu\nu}$, where η is the viscosity coefficient.

The shear tensor has the general form (Peitz & Appl 1997)

$$\sigma_{\mu\nu} = \frac{1}{2} \left[(u_{\mu;\gamma}h_\nu^\gamma + u_{\nu;\gamma}h_\mu^\gamma) - \frac{2}{3}\Theta_{\text{exp}}h_{\mu\nu} \right], \quad (2)$$

where $h_{\mu\nu} = g_{\mu\nu} + u_\mu u_\nu$ is the projection tensor, and $\Theta_{\text{exp}} = u_{;\gamma}^\gamma$ is expansion of the fluid world line. Equation (2) can be rewritten as

$$\sigma_{\mu\nu} = \frac{1}{2} \left[(u_{\mu;\nu} + u_{\nu;\mu} + a_\mu u_\nu + a_\nu u_\mu) - \frac{2}{3}\Theta_{\text{exp}}h_{\mu\nu} \right], \quad (3)$$

where $a_\mu = u_{\mu;\gamma}u^\gamma$ is the four-acceleration. The covariant derivative of covariant component of four-velocity is defined as $u_{\mu;\gamma} = u_{\mu,\gamma} - \Gamma_{\mu\gamma}^\beta u_\beta$, where $\Gamma_{\mu\gamma}^\beta$ is the Christoffel symbol. We

choose the geometric units where $G = M_{\text{bh}} = c = 1$ (G is the gravitational constant, M_{bh} is the mass of the BH), which has been used in all the equations, unless mentioned otherwise.

The governing equations of the relativistic fluid are

$$T_{;\nu}^{\mu\nu} = 0, \quad (\rho u^\nu)_{;\nu} = 0. \quad (4)$$

The relativistic Navier Stokes equation is obtained by projecting the energy momentum conservation along the i th direction i. e. $h_\mu^i T_{;\nu}^{\mu\nu} = 0$ ($i = 1, 2, 3$) and can be written as,

$$[(e + p)u^\nu u_{;\nu}^i + (g^{i\nu} + u^i u^\nu)p_{,\nu}] + h_\mu^i t_{;\nu}^{\mu\nu} = 0 \quad (5)$$

The energy generation equation or the first law of thermodynamics is $u_\mu T_{;\nu}^{\mu\nu} = 0$ and is given by,

$$u^\mu \left[\left(\frac{e + p}{\rho} \right) \rho_{,\mu} - e_{,\mu} \right] = Q^+, \quad (6)$$

where, $Q^+ = t^{\mu\nu} \sigma_{\mu\nu}$ is the viscous heating term and we ignore cooling terms, to stress on the effect of viscous dissipation. Here ρ is the mass density of the flow and h is the specific enthalpy of the flow,

$$h = \frac{e + p}{\rho}. \quad (7)$$

We have considered only the $r - \phi$ component of relativistic shear tensor. This would on one hand simplify the equations tremendously, and on the other hand would allow us to directly compare with the plethora of work done with pseudo potentials (Becker *et al.* 2008; Kumar & Chattopadhyay 2013; Kumar *et al.* 2014; Kumar & Chattopadhyay 2014). The $r - \phi$ component of the shear tensor (equation 3) is written as (Peitz & Appl 1997)

$$2\sigma_\phi^r = u_{;\phi}^r + g^{rr}u_{\phi;r} + a^r u_\phi + a_\phi u^r - \frac{2}{3}\Theta_{\text{exp}}u^r u_\phi. \quad (8)$$

Following Peitz & Appl (1997), we neglect derivatives of u^r, a^r and Θ_{exp} and equation (8) becomes

$$2\sigma_\phi^r = (g^{rr} + u^r u^r) \frac{du_\phi}{dr} - \frac{2u_\phi}{r} g^{rr}. \quad (9)$$

In this paper, we consider only the simplest BH metric for the accretion disc, namely the Schwarzschild metric, in which the non-zero metric components are

$$g_{tt} = - \left(1 - \frac{2}{r} \right); \quad g_{rr} = \left(1 - \frac{2}{r} \right)^{-1}; \quad g_{\theta\theta} = r^2; \quad g_{\phi\phi} = r^2 \sin^2 \theta.$$

For accretion, the flow is around the equatorial plane; therefore, the equations are obtained at $\theta = \pi/2$ and assumed hydrostatic equilibrium along the transverse direction. With these assumptions, we write down the radial component of Navier Stokes equation (5),

$$u^r \frac{du^r}{dr} + \frac{1}{r^2} - (r - 3)u^\phi u^\phi + (g^{rr} + u^r u^r) \frac{1}{e + p} \frac{dp}{dr} = 0, \quad (10)$$

the integrated form of the azimuthal component of equation (5),

$$-\rho u^r(L - L_0) = 2\eta\sigma_\phi^r, \quad (11)$$

where $L = hu_\phi = hl$ and L_0 are the local bulk angular momentum and bulk angular momentum at the horizon of the BH, respectively. It must be remembered that while $l = u_\phi$ is a conserved quantity in the absence of dissipation for particles, for fluid L is the corresponding conserved quantity. The specific angular momentum for fluid is therefore $\lambda = -u_\phi/u_t$, but for particles it is l or u_ϕ . Moreover, the radial three velocity is defined as $v_{\hat{r}}^2 = -(u_r u^r)/(u_t u^t)$ and in the local corotating frame $v^2 = \gamma_\phi^2 v_{\hat{r}}^2$ (Lu 1985). The associated Lorentz factors being $\gamma_v = (1 - v^2)^{-1/2}$, $\gamma_\phi = (1 - v_\phi^2)^{-1/2}$ and the total Lorentz factor is $\gamma = \gamma_v \gamma_\phi$. Moreover, $v_\phi = \sqrt{-u_\phi u^\phi / u_t u^t} = \sqrt{\Omega \lambda}$, where $\Omega = u^\phi / u^t$. The hydrostatic equilibrium along the transverse direction gives local disc height expression (Lasota 1994; Riffert & Herold 1995; Peitz & Appl 1997),

$$H = \left(\frac{pr^3}{\rho\gamma_\phi^2} \right)^{1/2}. \quad (12)$$

The first law of thermodynamics (equation 6)

$$u^r \left[\left(\frac{e+p}{\rho} \right) \rho_{,r} - e_{,r} \right] = t^{r\phi} \sigma_{r\phi} \quad (13)$$

Integrating mass-conservation equation, we obtain the expression of the mass accretion rate,

$$-\dot{M} = 4\pi\rho H u^r r. \quad (14)$$

We can now define the dynamical viscosity coefficient and it is $\eta = \rho\nu$, where the kinematic viscosity is given by $\nu = \alpha a r f_c$, a is the sound speed (see equation 23) and $f_c = (1 - v^2)^2$. Since $\sigma_{r\phi}$ may or may not be equal to zero on the horizon, with the choice of f_c we have made $t^{r\phi}|_{\text{horizon}} = 0$ (see Peitz & Appl 1997, for details).

The constant of motion can be obtained by integrating equation (10),

$$\log(E) = -\frac{1}{2}\log(1 - v^2) + \frac{1}{2}\log\left(1 - \frac{2}{r}\right) - \int \frac{(r-3)t^2}{r^3(r-2)\gamma_v^2} dr + \int \frac{1}{e+p} dp. \quad (15)$$

The last term of equation (15) with the help of equations (7) and (13) can be written as

$$\int \frac{1}{e+p} dp = \int \frac{1}{h} \frac{dp}{\rho} = \int \frac{1}{h} \left[dh - \frac{t^{r\phi} \sigma_{r\phi}}{\rho u^r} dr \right]. \quad (16)$$

Using equation (11) and relation $t^{r\phi} = -2\eta\sigma^{r\phi}$ in equation (16), we get,

$$\int \frac{1}{e+p} dp = \int \frac{1}{h} \left[dh + \frac{u^r(L - L_0)^2}{2\nu r(r-2)} dr \right]. \quad (17)$$

Combining equation (17) in equation (15) and re-arranging, we get

$$E = \frac{h\gamma_v \sqrt{1 - \frac{2}{r}}}{\exp(X_f)}, \quad (18)$$

where

$$X_f = \int \left[\left(\frac{r-3}{r-2} \right) \frac{l^2}{r^3 \gamma_v^2} - \frac{u^r (L - L_0)^2}{2\nu h r (r-2)} \right] dr.$$

E is the constant of motion in the presence of viscous dissipation and may be called the relativistic Bernoulli constant in the presence of viscosity. It is interesting to note that in the absence of viscosity, the first term in the parentheses of X_f is $\ln(\gamma_\phi^{-1})$, and so $E(\text{inviscid}) = h\gamma_v\gamma_\phi\sqrt{(1-2/r)} = -hu_t = \mathcal{E}$, i.e. the relativistic Bernoulli constant. It is indeed intriguing to note that E also has the same dimension of \mathcal{E} , i.e. of specific energy, but the former is a constant of motion while \mathcal{E} is not. It must be noted that \mathcal{E} incorporates the information of motion locally, i.e. motion along radial and azimuthal direction (quasi-one-dimensional), and the effect of gravity through $-u_t$, while the information of internal energy is through h . Therefore, \mathcal{E} contains the information of viscous heat dissipation (it increases where viscosity is effective), but not the angular momentum transport due to viscosity; as a result, it is not a constant of motion. However, E contains all the information carried by \mathcal{E} , as well as the information of angular momentum transport, which makes E constant. So it might be physically more relevant to consider E as the specific energy for dissipative flow than \mathcal{E} . Since specific energy expression in GR is not additive, so all the terms are not apparent; however, a comparison of the constants of motion for dissipative and inviscid Newtonian flow might be instructive. From Gu & Lu (2004); Becker *et al.* (2008) and Kumar & Chattopadhyay (2013, 2014), one may write down the grand specific energy or generalized Bernoulli parameter for Newtonian fluid as

$$E(\text{pNp}) = \frac{1}{2}v_{\text{pNp}}^2 + h_{\text{pNp}} - \frac{\lambda_{\text{pNp}}^2}{2r^2} + \frac{\lambda_{\text{pNp}}\lambda_{0\text{pNp}}}{r^2} - \frac{1}{2(r-1)}. \quad (\text{A})$$

The canonical Bernoulli parameter for Newtonian fluid is

$$\mathcal{E}(\text{pNp}) = \frac{1}{2}v_{\text{pNp}}^2 + h_{\text{pNp}} + \frac{\lambda_{\text{pNp}}^2}{2r^2} - \frac{1}{2(r-1)}. \quad (\text{B})$$

In the above, the suffix pNp denotes that the flow variables are in pNp regime, $\lambda_{0\text{pNp}}$ is the specific angular momentum at r_g and the last term on r.h.s of both the equations (A and B) is the gravity term in pNp. It is clear that while $\mathcal{E}(\text{pNp})$ contains the local information of radial motion (first term), azimuthal motion (λ_{pNp}), gravity and the thermal (h_{pNp}) terms, E contains all of them, as well as the angular momentum transport term (third and fourth terms of equation A). Clearly, if there is no viscosity, then $\lambda_{0\text{pNp}} = \lambda_{\text{pNp}}$, so $E(\text{pNp}) \rightarrow \mathcal{E}(\text{pNp})$. Therefore, one may say E in equation (18) is the constant of motion for viscous, relativistic fluid, equivalent to the one obtained in the pseudo-Newtonian limit (e.g., Gu & Lu 2004; Kumar & Chattopadhyay 2013, 2014).

2.2 Relativistic EoS and the equations of motion:

To solve the equations of motion, we need a closure relation between thermodynamic quantities called the EoS. In this subsection, we will start by expressing the variables in physical units, and at the end while applying into equations of motion we will impose the geometric units. We consider that the fluid is composed of electrons (e^-), positrons (e^+) and protons (p^+) of varying proportions, but always maintaining the overall charge neutrality: $n_{e^-} = n_{p^+} + n_{e^+}$, here n_s is the number density of the s th species of the fluid. The mass density is given by Chattopadhyay (2008) and Chattopadhyay & Ryu (2009),

$$\rho = \sum_i n_i m_i = n_{e^-} m_{e^-} [2 - \xi(1 - 1/\chi)] = n_{e^-} m_{e^-} \tilde{\tau}, \quad (19)$$

where, $\chi = m_{e^-}/m_{p^+}$, $\xi = n_{p^+}/n_{e^-}$ is the composition parameter and $\tilde{\tau} = [2 - \xi(1 - 1/\chi)]$. The electron and proton masses are m_{e^-} and m_{p^+} , respectively. For single temperature flow, the isotropic pressure is given by

$$p = \sum_i p_i = 2n_{e^-} kT = 2n_{e^-} m_{e^-} c^2 \Theta = \frac{2\rho c^2 \Theta}{\tilde{\tau}}. \quad (20)$$

The EoS for multi-species flow is (Chattopadhyay 2008; Chattopadhyay & Ryu 2009)

$$e = \sum_i e_i = \sum \left[n_i m_i c^2 + p_i \left(\frac{9p_i + 3n_i m_i c^2}{3p_i + 2n_i m_i c^2} \right) \right]. \quad (21)$$

The non-dimensional temperature is defined with respect to the electron rest mass energy, $\Theta = kT/(m_{e^-} c^2)$. Using equations (19) and (20), the expression of the energy density in equation (21) simplifies to

$$e = n_{e^-} m_{e^-} c^2 f = \rho_{e^-} c^2 f = \frac{\rho f}{\tilde{\tau}}, \quad (22)$$

where

$$f = (2 - \xi) \left[1 + \Theta \left(\frac{9\Theta + 3}{3\Theta + 2} \right) \right] + \xi \left[\frac{1}{\chi} + \Theta \left(\frac{9\Theta + 3/\chi}{3\Theta + 2/\chi} \right) \right].$$

The expressions of the polytropic index, the adiabatic index and the sound speed are given as,

$$N = \frac{1}{2} \frac{df}{d\Theta}; \quad \Gamma = 1 + \frac{1}{N}, \quad \text{and} \quad a^2 = \frac{\Gamma p}{e + p} = \frac{2\Gamma\Theta}{f + 2\Theta}. \quad (23)$$

Integration of first law of thermodynamics (equation 13) by assuming adiabatic flow ($Q^+ = 0$) and using the EoS (equation 22), gives us the adiabatic relation of multi-species relativistic flow (Chattopadhyay & Kumar 2013; Kumar *et al.* 2013),

$$\rho = \mathcal{K} \exp(k_3) \Theta^{3/2} (3\Theta + 2)^{k_1} (3\Theta + 2/\chi)^{k_2}, \quad (24)$$

where $k_1 = 3(2 - \xi)/4$, $k_2 = 3\xi/4$ and $k_3 = (f - \tilde{\tau})/(2\Theta)$ and \mathcal{K} is the constant of entropy. Equation (24) is the generalized version of $p = \mathcal{K}\rho^\Gamma$. Combining equations (24) and (14), we

get the expression of entropy accretion rate,

$$\dot{\mathcal{M}} = \frac{\dot{M}}{4\pi\mathcal{K}} = \exp(k_3)\Theta^{3/2}(3\Theta + 2)^{k_1}(3\Theta + 2/\chi)^{k_2}Hru^r. \quad (25)$$

Re-arranging equations (10-14) with the help of equations (9), (7), (19), (20) and (22) in geometric units, we present the spatial derivative of flow variables v, l and Θ ,

$$\frac{dv}{dr} = \frac{\mathcal{N}}{\mathcal{D}}, \quad (26)$$

where

$$\begin{aligned} \mathcal{N} &= -\frac{1}{r(r-2)} + \left(\frac{r-3}{r-2}\right)\frac{l^2}{r^3\gamma_v^2} + \frac{2a^2}{\Gamma+1} \\ &\times \left[\frac{\tilde{\tau}u^r(L-L_0)^2}{8\nu r(r-2)(N+1)\Theta} + \frac{5r-8}{2r(r-2)} - \frac{l^2}{r^2\gamma^2} \left(\frac{1}{l} \frac{dl}{dr} - \frac{1}{r} \right) \right] \\ \mathcal{D} &= \gamma_v^2 \left[v - \frac{2a^2}{\Gamma+1} \left(\frac{l^2}{r^2\gamma^2} v + \frac{1}{v} \right) \right]. \end{aligned}$$

Here, \mathcal{D} contains an extra term $l^2v/(r^2\gamma^2)$ compared to the inviscid case (Chattopadhyay & Chakrabarti 2011). There is γ_ϕ term in the expression of disc height (equation 12). The radial derivative of equation (14) implies that the radial derivative of the specific angular momentum will be non-zero, which causes the extra term to appear. There are many height prescriptions (Lasota 1994; Riffert & Herold 1995; Peitz & Appl 1997), and choice of any one of them apart from the one used, will not affect the result qualitatively. Then,

$$\frac{dl}{dr} = \left[-\frac{u^r(L-L_0)}{\nu(1-\frac{2}{r})} + \frac{2l}{r} \right] (1-v^2). \quad (27)$$

Moreover,

$$\begin{aligned} \frac{d\Theta}{dr} &= -\frac{\tilde{\tau}u^r(L-L_0)^2}{2\nu r(r-2)(2N+1)} - \frac{2\Theta}{2N+1} \\ &\times \left[\frac{5r-8}{2r(r-2)} + \gamma_v^2 \left(\frac{1}{v} + v \frac{l^2}{r^2\gamma^2} \right) \frac{dv}{dr} - \frac{l^2}{r^2\gamma^2} \left\{ \frac{1}{l} \frac{dl}{dr} - \frac{1}{r} \right\} \right]. \end{aligned} \quad (28)$$

These differential equations are integrated by using fourth order Runge Kutta numerical method with the help of using critical point conditions and l'Hospital rule at critical point.

2.2.1 Sonic point equations

Mathematical form of critical point equation is $dv/dr = \mathcal{N}/\mathcal{D} = 0/0$, which gives two equations as,

$$\left[1 - \frac{2}{\Gamma_c + 1} \left(\frac{a_c^2 l_c^2}{r_c^2 \gamma_c^2} + \frac{a_c^2}{v_c^2} \right) \right] = 0 \quad (29)$$

and

$$-\frac{1}{r_c(r_c-2)} + \left(\frac{r_c-3}{r_c-2}\right) \frac{l_c^2}{r_c^3 \gamma_{v_c}^2} + \frac{2a_c^2}{\Gamma_c+1} \quad (30)$$

$$\times \left[\frac{\tilde{\tau} u_c^r (L_c - L_0)^2}{8\nu_c r_c (r_c - 2) N_c \Gamma_c \Theta_c} + \frac{5r_c - 8}{2r_c(r_c - 2)} + \frac{l_c^2}{r_c \gamma_c^2} \left(\frac{u_c^r (L_c - L_0)}{\nu_c l_c \gamma_{v_c}^2 (r_c - 2)} - \frac{1 - 2v_c^2}{r_c^2} \right) \right] = 0.$$

Here, the subscript ‘c’ denotes the same physical quantities described in equations (26-28), but evaluated at the location of the critical point. The velocity gradient on the sonic point, i.e. $(dv/dr)_c$, is obtained by employing l’Hospital rule.

2.2.2 Relativistic shocks for viscous flow

The relativistic shock conditions were first obtained by Taub (1948), which for viscous flow in the presence of mass-loss are

$$\dot{M}_+ = \dot{M}_- - \dot{M}_o \quad (31)$$

$$[\Sigma h \gamma_v^2 v v + W] = 0 \quad (32)$$

$$[\dot{J}] = 0 \quad (33)$$

$$[\dot{E}] = 0 \quad (34)$$

where, $\dot{J} = \dot{M} L_0 = \dot{M}(L - 2\nu\sigma_\phi^r/u^r)$, $\dot{E} = \dot{M}E$, $\Sigma = 2\rho H$ and $W = 2pH$. We have solved four shock conditions (31-34) simultaneously, where viscous shear tensor (σ_ϕ^r) is continuous across the shock and we obtained the relation between pre-shock (suffix ‘-’) and post-shock (suffix ‘+’) flow variables,

$$L_- = L_+ + (2\sigma_\phi^r|_+) \left[\frac{\nu_+}{u_+} - \frac{\nu_-}{u_-} \right]; \quad h'_- u_-^2 - k_1 u_- + 2\Theta_- = 0; \quad k_2 - \exp(X_{f-}) h'_- \gamma_{v-} = 0, \quad (35)$$

where, $k_1 = (1 - R_{\dot{m}})(h'_+ u_+^2 + 2\Theta_+)/u_+$, $R_{\dot{m}} = \dot{M}_o/\dot{M}_-$, $k_2 = \exp(X_{f+}) h'_+ \gamma_{v+}$, $h' = (f + 2\Theta)$ and $u = v\gamma_v$. Here, $X_{f-} = (f_l/f_\gamma)^2 X_{l+} + f_u f_L^2 X_{L+}/(f_\nu f_h)$, $X_{l+} = \int (\frac{r-3}{r-2}) \frac{l_+^2}{r^3 \gamma_{v+}^2} dr$, $X_{L+} = -\int \frac{u_+^r (L_+ - L_0)^2}{2\nu_+ h_+ r (r-2)} dr$, $f_l = l_-/l_+$, $f_\gamma = \gamma_{v-}/\gamma_{v+}$, $f_u = u_-^r/u_+^r$, $f_L = (L_- - L_0)/(L_+ - L_0)$, $f_\nu = \nu_-/\nu_+$, $f_h = h_-/h_+$, and $X_{f+} = X_{l+} + X_{L+}$. From equation (11), viscous shear tensor can be written as $2\sigma_\phi^r|_+ = -u_+(L_+ - L_0)/\nu_+$.

2.3 Outflow equations

The jet being tenuous, we idealize it to be inviscid; therefore, the energy momentum tensor of jet fluid should be ideal. The general form of the equations of motion would be similar

(equation 4); however, the geometry is entirely different (see Fig. 1). For the jet we define,

$$\vartheta^i = \frac{u_j^i}{u_j^t} \quad \text{and} \quad \vartheta_i = -\frac{u_{ij}}{u_{tj}}, \quad (36)$$

where $i = (r, \theta, \phi)$ and ‘j’ implies jet quantities and should not be confused with vector or tensor components. Here, ϑ^i and ϑ_i are the component of ‘transport’ velocity (also called as coordinate velocity) and the respective momentum per unit inertial mass (Chakrabarti 1985). The azimuthal three-velocity of the jet is defined as $v_{\phi j} = (\vartheta_\phi \vartheta^\phi)^{1/2} = (\Omega_j \lambda_j)^{1/2}$, where λ_j , the specific angular of the jet, is constant along the flow. The three-velocity of the jet along the stream line is given by $v_p^2 = \vartheta_r \vartheta^r + \vartheta_\theta \vartheta^\theta$. The surfaces of constant angular momentum for jets in GR are VZS where the von Zeipel parameter is constant (Kozłowski et. al. 1978; Chakrabarti 1985). The von Zeipel parameter is defined as

$$Z_\phi = \left(\frac{\vartheta_\phi}{\vartheta^\phi} \right)^{1/2} = \left(-\frac{g^{tt}}{g^{\phi\phi}} \right)^{1/2} = \frac{r_j \sin \theta_j}{(1 - 2/r_j)^{1/2}}. \quad (37)$$

Equation (37) defines the streamline. The angular momentum of jets would be related to the von Zeipel parameter (Chakrabarti 1985)

$$\vartheta_\phi = c_\phi Z_\phi^n, \quad (38)$$

where c_ϕ and n are some constant parameters. Using equation (38) along with EoS (equation 22), the definitions of h (equation 7) and Z_ϕ (equation 37) while integrating the jet equations of motion gives us the constant of motion of the jet, which is similar to the Bernoulli parameter along the streamline of the jet,

$$\mathfrak{R}_j = -h_j u_{tj} [1 - c_\phi^2 Z_\phi^{(2n-2)}]^\beta, \quad (39)$$

where $u_{tj} = -(1 - 2/r_j)^{1/2} \gamma_j$, $\gamma_j = \gamma_{vj} \gamma_{\phi j}$, $\gamma_{vj} = 1/\sqrt{(1 - v_j^2)}$, $\gamma_{\phi j} = 1/\sqrt{(1 - c_\phi^2 Z_\phi^{(2n-2)})}$, $v_j = \gamma_{\phi j} v_p$ and $\beta = n/(2n - 2)$. The mass outflow equation can be written as,

$$\dot{M}_o = \rho_j u_j^p \mathcal{A}_j, \quad (40)$$

where $\rho_j, u_j^p = \sqrt{g^{pp}} \gamma_{vj} v_j$ and \mathcal{A}_j are jet mass density, jet four-velocity along the VZS and area of jet cross-section, respectively. The expression of $g^{pp} = 1/h_p^2$ is defined in Appendix A. And similar to the accretion disc equations, we can also derive the entropy-outflow rate for the jet, and is defined as

$$\dot{\mathcal{M}}_j = \frac{\dot{M}_o}{2\pi \mathcal{K}} = \exp(k_3) \Theta_j^{3/2} (3\Theta_j + 2)^{k_1} (3\Theta_j + 2/\chi)^{k_2} u_j^p \frac{\mathcal{A}_j}{2\pi}. \quad (41)$$

If there are no shocks in jets, then $\dot{\mathcal{M}}_j$ will remain constant along the streamline. The differential form of equation (39) with the help of equations (40) and (24) and after some

manipulations is obtained as

$$\frac{dv_j}{dr_j} = \frac{\frac{a_j^2}{\mathcal{A}_j} \frac{d\mathcal{A}_j}{dr_j} - \frac{a_j^2}{h_p} \frac{dh_p}{dr_j} - \frac{1}{r_j(r_j-2)}}{v_j \gamma_{vj}^2 [1 - \frac{a_j^2}{v_j^2}]} = \frac{\mathcal{N}_j}{\mathcal{D}_j} \quad (42)$$

and

$$\frac{d\Theta_j}{dr_j} = -\frac{\Theta_j}{N_j} \left[\frac{\gamma_{vj}^2}{v_j} \frac{dv_j}{dr_j} + \frac{1}{\mathcal{A}_j} \frac{d\mathcal{A}_j}{dr_j} - \frac{1}{h_p} \frac{dh_p}{dr_j} \right]. \quad (43)$$

Here, expression of \mathcal{A}_j is defined in equation (50) in Section 3.3. It is to be noted that $(d\mathcal{A}_j)/(\mathcal{A}_j dr_j) = (r_j - 1)/[r_j(r_j - 2)]$ and $(dh_p)/(h_p dr_j) = (dh_1)/(h_1 dr_j) - (dh_2)/(h_2 dr_j) - \tan\theta_j(d\theta_j/dr_j) - 1/[r_j(r_j - 2)]$. Here, $h_1 = 1 + \tan^2\theta_j(r_j - 3)^2/[r_j(r_j - 2)]$, $h_2 = h_3^2 + h_4^2 \tan^4\theta_j(r_j - 3)^2/(r_j - 2)^2$, $dh_1/dr_j = -\theta'_j \tan\theta_j[(6 - r_j)/r_j + (r_j - 3)\theta'_j \tan\theta_j]$, $dh_2/dr_j = h_3(2 - \sin 2\theta_j \theta'_j) + h_4(r_j - 3) \tan^4\theta_j[(r_j - 3)\{1 + (\sin 2\theta_j + 4h_4/\sin 2\theta_j)\theta'_j\} + h_4/(r_j - 2)]/(r_j - 2)^2$, $h_3 = (2r_j - 2 - \sin^2\theta_j)$, $h_4 = (r_j - 4 + \sin^2\theta_j)$ and from differentiation of eq. (37), we get $d\theta_j/dr_j = \theta'_j = -\tan\theta_j(r_j - 3)/[r_j(r_j - 2)]$.

2.3.1 Jet sonic point

From the definitions, jet critical point conditions are obtained from equations (42) and (43) as,

$$\mathcal{N}_j = 0 \quad \Rightarrow \quad a_{jc}^2 = \frac{1/[r_{jc}(r_{jc} - 2)]}{[\frac{1}{\mathcal{A}_{jc}} \frac{d\mathcal{A}_{jc}}{dr_{jc}} - \frac{1}{h_p} \frac{dh_p}{dr_j}]}, \quad (44)$$

and

$$\mathcal{D}_j = 0 \quad \Rightarrow \quad M_{jc}^2 = \frac{v_{jc}}{a_{jc}}, \quad (45)$$

where, subscript ‘c’ denotes flow values at critical point. And the velocity gradient at the critical point is obtained by l’Hospital’s rule.

3 SOLUTION PROCEDURE

We first solve for the accretion solution and once the accretion solution is obtained, we iteratively find the jet solution from the accretion solution. Since, close to the horizon, gravity dominates all other physical processes, so the infall time-scale of matter will be smaller than viscous time-scale or any other time-scales. In other words, very close to the horizon, matter is almost falling freely and $E \simeq \mathcal{E}$. It may be remembered from Section 2.1 that E is the generalized relativistic Bernoulli parameter in the presence of viscosity and \mathcal{E} is the canonical relativistic Bernoulli parameter. In steady state, for inviscid flow \mathcal{E} is a

constant of motion and for viscous flow E is a constant of motion. Therefore, at a distance $r_{\text{in}} \rightarrow r_g$, $v_{\text{in}} = \delta\sqrt{2/r_{\text{in}}}$. Here, $r_g = 2r_s = 2GM_B/c^2$, $r_{\text{in}} = 2.001r_s$ and $\delta < 1$. We start by assigning $\delta = 1$ in v_{in} , and obtain Θ_{in} and L_0 . With these values, we integrate equations (26), (27) and (28) outwards. If the ensuing solution does not satisfy critical point conditions (equations 29 and 30), we reduce δ and repeat the procedure till the accretion critical points are obtained and thereby fixing the value of δ .

3.1 Method to find L_0

We have provided four flow parameters (E, ξ, α and λ_{in} or L_{in}) and by using v_{in} , we can calculate Θ_{in} from relativistic Bernoulli equation $\mathcal{E} = -hu_t$. Since we know $u_t [= -\sqrt{(1-2/r)} \gamma]$ from v_{in} , λ_{in} and $E = \mathcal{E}$ at $r = r_{\text{in}} = 2.001r_s$, so enthalpy (h) can be expressed as cubic equation in Θ from enthalpy equation (7), which is

$$X_3\Theta^3 + X_2\Theta^2 + X_1\Theta + X_0 = 0, \quad (46)$$

where, $X_3 = 72\chi$, $X_2 = 3[16(\chi + 1) - 3\chi\tilde{\tau}X_c]$, $X_1 = 2[10 - 3\tilde{\tau}(X_c - 1)(\chi + 1)]$, $X_0 = -4\tilde{\tau}(X_c - 1)$ and $X_c = -\mathcal{E}/u_t$. Equation (46) gives three real roots but two are negative and only one is positive, so we used positive root and is symbolized as Θ_{in} . Now, L_0 can be calculated from equation (18) by assuming $E = \mathcal{E}$ at r_{in} . Since we assume $E = \mathcal{E} = -hu_t$ close to the horizon, therefore, from equation (18) at $r = r_{\text{in}}$ we have $\gamma_\phi \exp(X_f) = 1$. This condition is written as,

$$-\frac{1}{\gamma_\phi} \frac{d\gamma_\phi}{dr} = \left[\left(\frac{r-3}{r-2} \right) \frac{l^2}{r^3\gamma_v^2} - \frac{u^r(L-L_0)^2}{2\nu hr(r-2)} \right]. \quad (47)$$

Simplifying the above equation with the help of equations (26) and (27), we get a quadratic equation in L_0 , given by

$$b_2L_0^2 + b_1L_0 + b_0 = 0, \quad (48)$$

where, $b_2 = u^r[\tilde{\tau}vv_\phi^2\wp/(4\Theta D N\Gamma) + 1/h]/[2\nu r(r-2)]$, $b_1 = -2L_{\text{in}}b_2 - a_1$ and $b_0 = b_2L_{\text{in}}^2 + a_1L_{\text{in}} + a_0$. Here, $a_1 = [u^rv_\phi^2(v - \wp/v)]/[\nu\gamma_v^2l(1-2/r)D]$, $a_0 = vv_\phi^2[-1 + (5r-8)\wp/2 + (r-3)\gamma_\phi^2\wp(v_\phi^2 + 1/v^2) + (r-2)(1-\wp/v^2)(1-2/\gamma_\phi^2)]/[r(r-2)D]$, $\wp = 2a^2/(\Gamma+1)$ and $D = [v - \wp(v_\phi^2v + 1/v)]$. Equation (48) gives two real roots, one is greater than L_{in} and other less than L_{in} . Since viscosity transports angular momentum outward, so second root, which is less than L_{in} , is the correct solution.

To summarize, we have obtained asymptotic values of v_{in} and Θ_{in} at $r_{\text{in}} = 2.001$ and L_0 or λ_0 on the horizon by using three flow parameters, E, α, L_{in} and ξ to fix the EoS, so that

we can integrate equations (26 - 28) simultaneously outwards from r_{in} . It is to be noted that only correct values of v_{in} , Θ_{in} and L_0 will produce a transonic solution.

3.2 To find critical point and shock locations in disc

Initially, a tentative accretion solution is obtained without considering mass-loss from the disc. We obtain the transonic solution iteratively, i.e., to say, for a given set of $(E, \alpha, L_{\text{in}})$, there exists a unique set of v_{in} , Θ_{in} and L_0 which will pass through a certain critical point (r_c). Once we obtain r_c , we integrate outwards to obtain global solution. Gravity induces one sonic point or critical point. Rotation induces multiple sonic points. If the first sonic point obtained is close to the horizon, we call it inner sonic point r_{ci} . If the transonic solution is monotonic, then there are no other sonic points. Once we get one sonic point, we continue to search for other sonic points. Up to three sonic points can be obtained, in which the inner (r_{ci}) and the outer (r_{co}) sonic points are X-type and are physical sonic points as flow actually passes through these sonic points. The middle sonic point is unphysical because flow actually does not pass through it, since the $(dv/dr)_c$ at middle sonic point is complex. For viscous fluid, the middle sonic point is spiral type.

For flows going through r_{ci} , we check for the shock conditions equations (35), initially assuming $\dot{M}_0 = 0$, and compute the pre-shock flow variables (i.e. v_- , a_- , L_-). We integrate with v_- , a_- , L_- along the supersonic branch and check whether solution passes through the outer sonic point or r_{co} . The location of the jump r_{sh} , for which the supersonic branch starting with v_- , a_- , L_- goes through r_{co} is the shock location. When there is a shock, then the entropy of the flow through r_{co} is less than the entropy of the flow through r_{ci} , i.e. $\dot{\mathcal{M}}_o < \dot{\mathcal{M}}_i$.

3.3 To find jet critical point and mass outflow rate

While E ($/\mathcal{E}$) is the constant of motion along equatorial plane for viscous ($/\text{inviscid}$) accretion solution, however, away from the equatorial plane, the constant of motion is given by equation (39) which is constant along the jet stream-line defined by equation (37). Numerical simulations show that the post-shock disc is the jet base (Molteni *et al.* 1996b; Das *et al.* 2014). Numerical simulations also show that the angular momentum at the top of the PSD (the base of the jet) is about 20-30% less than from the equatorial plane, so without losing generality we consider at the base $\lambda_j = 2\lambda/3$, and the location of the jet base

$x_b = (r_{ci} + r_{sh})/2$. We estimate \mathfrak{R} at x_b on the disc surface and the jet is launched with the same modified Bernoulli parameter, i.e. $\mathfrak{R}_j = \mathfrak{R}(x_b)$. The modified Bernoulli parameter (\mathfrak{R}_j) depends on constants n and c_ϕ apart from its local flow variables. Interestingly, the entropy of the jet also depends on these two parameters. Keeping same \mathfrak{R}_j , but by changing n and c_ϕ , iteratively, we obtain the $\dot{\mathcal{M}}_j$ which admits the transonic jet solutions, with the help of equations (44) and (45) for particular values of $n > 0$. Since only a fraction of matter escapes as jets, so $\dot{\mathcal{M}}_j$ should be less than local disc entropy at x_b but greater than the disc pre-shock entropy. Following the above constraint, c_ϕ and n would be related by $c_\phi = Z_\phi^n/\lambda_j$.

Once we know the jet solution it is easy to define the relative mass outflow rate,

$$R_{\dot{m}} = \frac{\dot{M}_0}{\dot{M}_-} = \frac{1}{[\dot{M}_+/\dot{M}_0 + 1]}. \quad (49)$$

The jet base cross-sectional area, perpendicular to tangent of the stream line at r_j is,

$$\mathcal{A}_j = \mathcal{A}_b \left(\frac{r_j}{r_b} \right)^2 \sin \theta_j, \quad (50)$$

where, $\mathcal{A}_b = \mathcal{A}'_b \sin \theta_b$ and $\mathcal{A}'_b = 2\pi(r_{b0}^2 - r_{bi}^2)$ are area along the accretion cylindrical radial coordinate and area along the spherical radial coordinate, respectively. Here, $r_b = \sqrt{x_b^2 + h_b^2}$, $\theta_b = \sin^{-1}(x_b/r_b)$, $r_{bi} = x_{bi}/\sin \theta_b$, $r_{b0} = x_{b0}/\sin \theta_b$, $x_b = (r_{ci} + r_{sh})/2$, $x_{bi} = r_{ci}$ and $x_{b0} = r_{sh}$. Here, $\theta_j = \sin^{-1}(Z_\phi \sqrt{1 - 2/r_j}/r_j)$ and $Z_\phi = r_b \sin \theta_b / \sqrt{(1 - 2/r_b)}$. Now the equation (49) with the help of equations (50), (40) and (14) can be written as,

$$R_{\dot{m}} = \frac{1}{[(4\pi H_+ r_+ \rho_+ u_+^r)/(\mathcal{A}_{jb} \rho_{jb} u_{jb}^p) + 1]} \quad (51)$$

$$= \frac{1}{[\Sigma(R_A R \Xi)^{-1} + 1]},$$

where $\rho_{jb} = \rho_b \exp(-7x_b/(3h_b))/h_b^2$, $u_{jb}^p = \sqrt{g^{pp}} \gamma_{vb} v_{jb}$ and $\mathcal{A}_{jb} = \mathcal{A}_b \sin \theta_b$ are jet base density, four-velocity at jet base and jet base area, respectively. Moreover, $R_A = \mathcal{A}_{jb}/(4\pi H_+ r_+)$, $R = (u_-^r)/(u_+^r)$ the compression ratio, $\Sigma = \rho_+/\rho_-$ o, the density jump across the accretion shock and $\Xi = (\rho_{jb} u_{jb}^p)/(\rho_- u_-^r)$ or the ratio of the relativistic mass flux of the pre-shock accretion flow and the jet base, respectively. It is to be noted that Ξ measures the upward thrust imparted by the shock through the compression ratio.

Once the jet solution is obtained for a particular accretion shock solution, we compute the relative mass outflow rate or $R_{\dot{m}}$, and feed it back to the shock conditions (equation 35) and retrace the steps mentioned in Sections 3.1 and 3.2 to find a new r_{sh} . Then from this new r_{sh} we find a new jet solution and new $R_{\dot{m}}$ (Section 3.3). We continue these iterations till

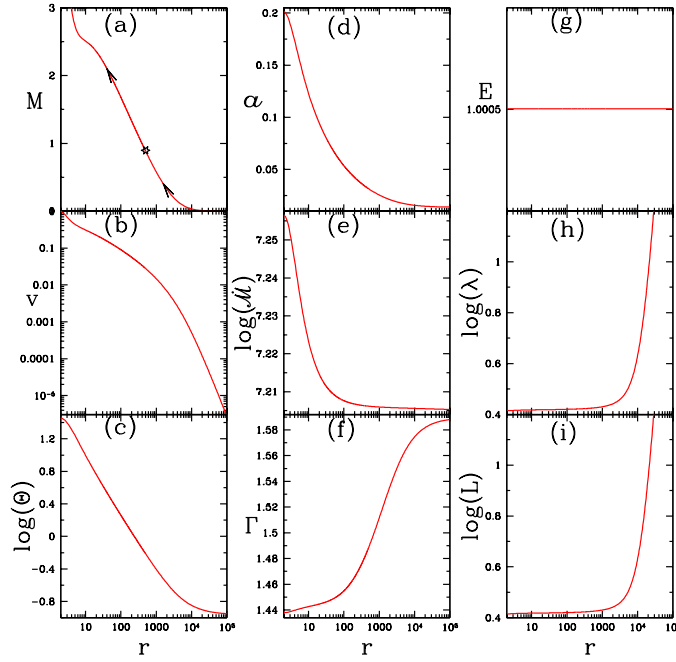


Figure 2. Variation of accretion Mach number M (a), bulk velocity v (b), dimensionless temperature Θ (c), sound speed a (d), entropy accretion rate $\dot{\mathcal{M}}$ (e), accretion adiabatic index Γ (f), generalized relativistic Bernoulli parameter E (g), specific angular momentum λ (h) and bulk angular momentum L (i). The sonic point is indicated by the star mark in panel (a). The accretion disc parameters are $E = 1.0005$, $L_0 = 2.6$, $\alpha = 0.01$ and $\xi = 1.0$.

the shock location converges and then we obtain a self-consistent accretion-ejection solution around BHs in full general relativistic regime.

4 RESULTS

In this paper, we obtained jet solution from accretion solutions. In other words, we supplied accretion disc parameters E, α, L_{in} and ξ to fix the EoS of the relativistic flow, obtained accretion and jet solutions simultaneously. However, in the following subsection we will first present all possible accretion solution and then in the next subsection we will present the accretion-ejection solutions. The location of the outer boundary of the accretion disc is $10^5 r_g$ for totally sub-Keplerian disc and/or wherever the angular momentum distribution achieves the local Keplerian value.

4.1 Inflow solutions

In Fig.(2), we plot the accretion solution for $E = 1.0005$, $L_0 = 2.6$, $\alpha = 0.01$. We choose $\xi = 1.0$, until specified otherwise. Various flow variables plotted are the Mach number $M = v/a$ (a), v (b), Θ (c), a (d), $\dot{\mathcal{M}}$ (e), Γ (f), E (g), λ (h) and L (i). The disc parameters were such that it produces a single outer-type sonic point. While Γ varies from semi-relativistic

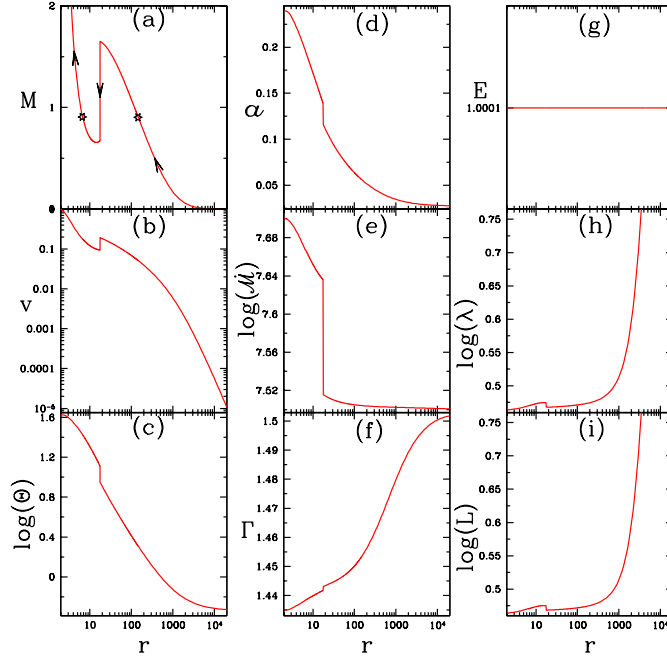


Figure 3. Variation of accretion Mach number M in plot (a), bulk velocity v in plot (b), dimensionless temperature Θ in plot (c), local sound speed a in plot (d), entropy accretion rate \dot{M} in plot (e), accretion adiabatic index Γ in plot (f), general relativistic Bernoulli parameter E in plot (g), specific angular momentum λ in plot (h) and bulk angular momentum L in plot (i) are shown in this figure. Here, vertical jump shows the location of shock, which is $r_s = 51.19$ and the two star marks in panel (a) indicate the X-type sonic points. The accretion disc parameters are $E = 1.0001$, $L_0 = 2.91$, $\alpha = 0.01$ and $\xi = 1.0$.

to relativistic values ($1.437 < \Gamma < 1.59$), the constant of motion E is indeed a constant. The entropy also increases due to viscous dissipation. And the angular momentum is transported outwards.

In Fig.(3), we have shown typical shocked accretion solution and variation of various flow quantities with radial distance, for a different value of E ($= 1.0001$) and L_0 ($= 2.91$) while keeping the viscosity and the nature of the fluid similar to the previous figure. Since E is a constant of motion in the viscous relativistic disc, and L_0 is a constant of integration, so changing these two disc parameters is equivalent to changing the inner boundary condition of the accreting flow. It is to be noted that, the solution in Fig. (2) is similar to a Bondi type solution (i.e. low angular momentum flow through an outer critical point r_{co} ; see Bondi 1952). So accretion flow is not decidedly monotonic or shocked, it depends on the boundary condition of the flow.

In Fig. (4), we obtain a parameter space of E and L_0 for $\alpha = 0.01$ and $\xi = 1$, and demarcate the regions which will give transonic solutions with single sonic points, multiple sonic points and shocked solutions. For all E , L_0 values in the domain ABD' , angular momentum is low and all possible solutions in this domain will possess a single outer-type sonic point similar to Bondi flow (typical Mach number variation: panel a). The region $BGFB$

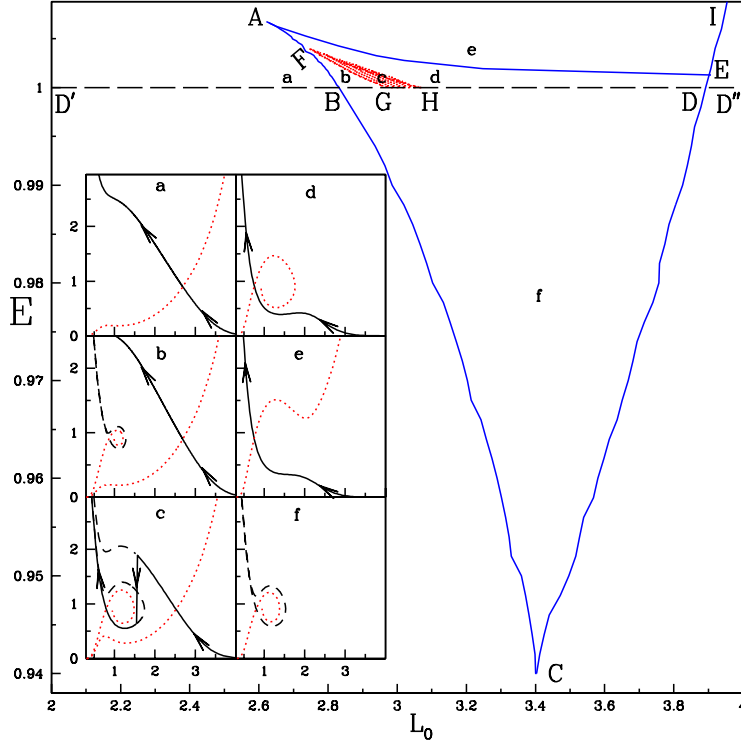


Figure 4. Division of parameter space (E, L_0) on the basis of number of critical points and corresponding solutions topologies [Mach number, M , versus radial distance, $\log(r)$ plots in panels a, b, c, d, e and f]. In this figure viscosity parameter, $\alpha = 0.01$ and composition parameter, $\xi = 1.0$.

is with a bit more angular momentum and the inner sonic point (r_{ci}) appears, although the accreting matter still flows through r_{co} into the BH (typical solution: panel b). Since the entropy of r_{ci} is higher for these values of E and L_0 , so oscillating shock is a distinct possibility. Solutions in the domain GFHG admit steady-state shock in accretion solutions and thereby joining the solutions through outer and inner sonic points (typical solution: panel c). In the domain HFADEH, the angular momentum is much higher, multiple sonic points still exist, but the accreting matter prefers to flow into the BH through r_{ci} because $\dot{\mathcal{M}}_i > \dot{\mathcal{M}}_o$ (typical solution: panel d). For solutions from the region AEI, the angular momentum is so large that matter falls with very low inflow velocity, and becomes transonic only close to the horizon, and therefore possess an inner-type sonic point only (typical solution: panel e). Solutions from the domain BDCB are bound through out and do not produce global transonic solutions (typical solution: panel f). The solid curves within panels (a) — (f) indicate physical solutions, which accreting matter actually follows. The dashed part of the solution indicates those which are viable solutions but matter do not choose. The dotted curves in the panels show also transonic solutions which have wind-type boundary conditions (low v close to horizon and high v at large distances). However, these so-called wind-type

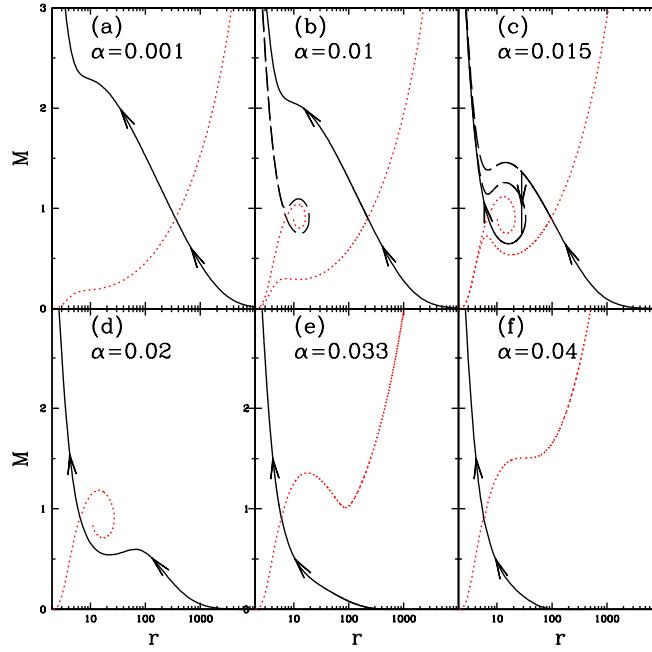


Figure 5. Variation of M with r for different viscosity parameters marked in each panel. For all panels, $E = 1.001$, $L_0 = 2.85$, and $\xi = 1.0$.

solutions should not be confused with proper wind or outflow solutions, since these solutions are defined only on the equatorial plane.

All possible accretion solutions can also be produced even if the viscosity is varied for a given value of E , L_0 and ξ . In Fig. (5a), we obtain a Bondi-type solution for a low- L_0 and low-viscosity ($\alpha = 0.001$) solution. We know viscosity transports angular momentum outwards, but low α means the angular momentum remains low at the outer edge too. Such low angular momentum does not produce a strong centrifugal barrier and therefore produces a shock-free Bondi-type solution with a single, outer-type sonic point. Keeping the same inner boundary condition, we increase the viscosity to $\alpha = 0.01$ and multiple sonic points appear in Fig. (5b). Higher viscosity for the same values of L_0 implies higher angular momentum at larger distances. Gravity ensures a single sonic point; however, for higher angular momentum flow, the effect of gravity is impeded by rotation at distances of few tens of r_g , while gravity dominating at distances further away, and also very close to the horizon. This causes multiple sonic points to form. Increasing to $\alpha = 0.015$ and keeping the same inner boundary condition, steady accretion shock is obtained in Fig. (5c). Higher α also ensures even higher λ of the disc, thus enhancing the centrifugal barrier. This causes the supersonic matter to be slowed down and eventually forms a shock. For even higher viscosity $\alpha = 0.02$, the solution through the inner sonic point opens up as shown

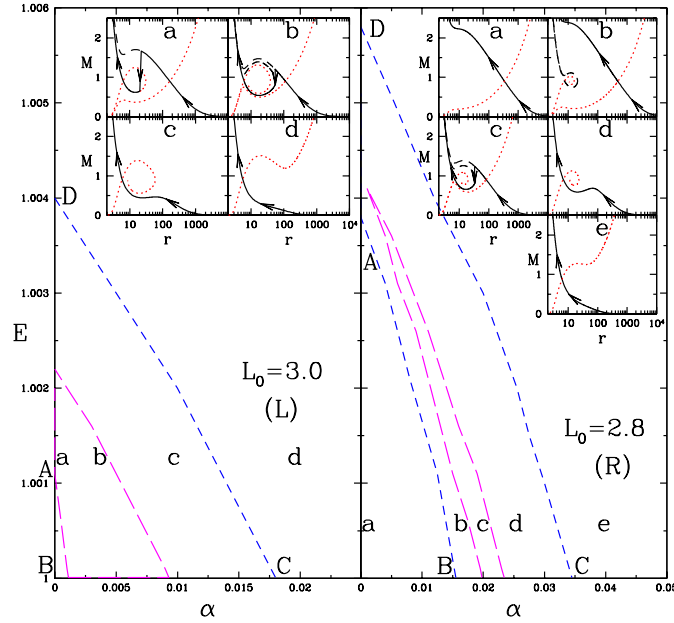


Figure 6. Parameter space of E and α for given values of $L_0 = 3$ (L) and $L_0 = 2.8$ (R). In the inset panels, solutions, i.e. \dot{M} versus r , are plotted, corresponding to the flow parameters (E and α) from various regions marked as a–e. In both the plots ABCDA is the region for multiple critical points.

in Fig. (5d). Increasing the viscosity even further, monotonic accretion solution is obtained (Figs. 5e, f). If the angular momentum increases beyond a certain limit, then the accreting matter becomes rotation dominated, and becomes supersonic only very close to the horizon. Therefore, accreting matter does not pass through outer sonic point (if present), and falls on to the BH through the inner sonic point. Hence, there exist two critical α for such boundary conditions, where the lower value of it would initiate the shock and the higher one will remove it. Such dependence of the nature of accretion solution on viscosity parameter have been studied in the pNp regime before (Chakrabarti 1996; Chattopadhyay & Das 2007; Kumar & Chattopadhyay 2013, 2014), but not in the GR regime.

In Fig. (6 L), we plot the parameter space of E and α for $L_0 = 3$ and various regions in the parameter space are marked as a—d and the typical solutions are plotted in the inset marked by the same alphabets. In Fig.(6R), we plot E and α for $L_0 = 2.8$ and various regions are marked as a—e, and the corresponding solutions are plotted in inset panels. Therefore, parameter space depicted in Figs. (6 L & R) is analogous to the parameter space depicted in Fig. (4), which pans all possible accretion solutions. It may be noted that the solutions for $\alpha = 0$ which harbour shocks also exhibit steady shocks up to moderate levels of α , but solutions which were Bondi type to start with for $\alpha = 0$, generate a shock transition above a critical value of α . For these kind of solutions, one can identify two critical viscosity

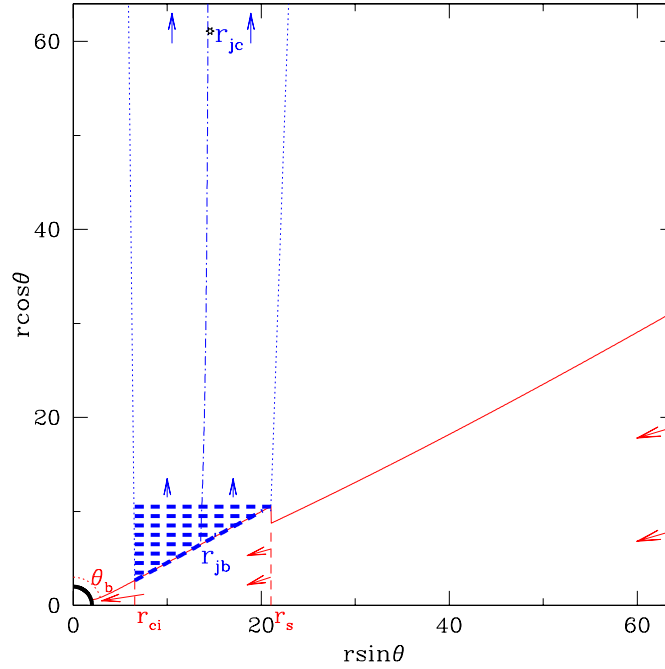


Figure 7. Typical accretion-jet flow geometry for accretion disc parameters $E = 1.0001$, $L_0 = 2.92$, $\alpha = 0.01$ and $\xi = 1$. Here solid (red) curve represents disc-half height. Dot-dashed (blue) line is jet stream-line for von Zeipel parameter $Z_\phi = 13.28$, and dotted (blue) line is the inner and outer boundary of jet flow cross-section. The jet sonic point is located at r_{jc} . Arrows represent direction of bulk motion and the solid thick quarter of a circle represents the event horizon.

parameters, one denotes the onset of steady shock, and the other which marks the limit above which no steady shock is obtained.

4.2 Outflow solutions

It has been shown in many simulations that the PSD drives bipolar outflows (Molteni *et al.* 1996a,b; Das *et al.* 2014), and in theoretical studies of simultaneous accretion-ejection model in the pNp regime, the flow geometry of the bipolar outflow or jet was considered within the two surfaces, one, centrifugal barrier surface (pressure maxima) and the other, funnel wall (minima of the effective potential), both described in the off-equatorial region (Chattopadhyay & Das 2007; Kumar *et al.* 2013, 2014). The problem is that both these surfaces depend primarily on the angular momentum of the flow, and therefore the outflow geometry depends poorly on the base of the jet or other factors of the flow, which should not be the case. In order to circumvent this as well as in GR, we were forced by correct physics to obtain the local outflow cross-section by identifying the relevant VZS, which is not bound by the limitations of pNp regime. In Fig. (7), we present the flow geometry of accretion disc, as well as bipolar jets which are actually solved self-consistently for accretion disc parameters $E = 1.0001$, $L_0 = 2.92$, $\alpha = 0.01$, where the disc half-height is plotted as

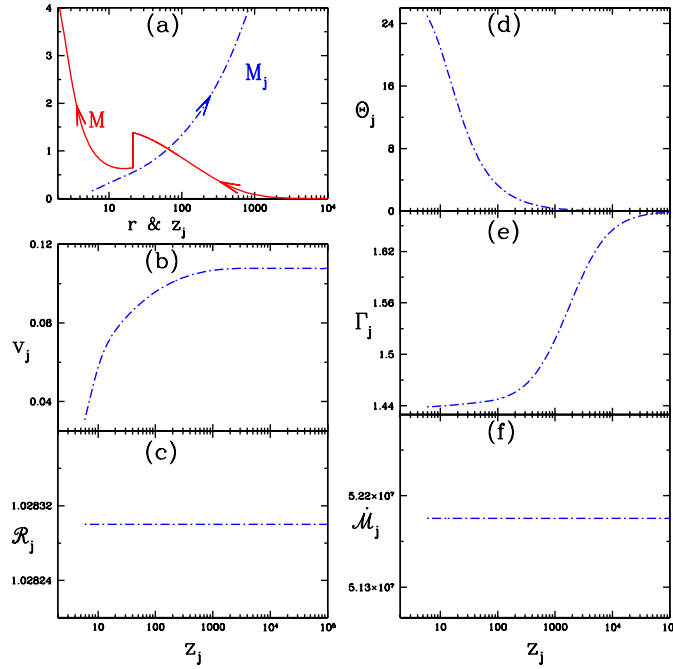


Figure 8. (a) Accretion Mach number M (solid) is plotted w.r.t r and jet Mach number M_j (dashed-dot) is plotted w.r.t z_j ; (b) variation jet 3-velocity v_j ; (c) jet Bernoulli parameter \mathcal{R}_j ; (d) jet dimensionless temperature Θ_j ; (e) jet adiabatic index Γ_j and (f) jet entropy ($\dot{\mathcal{M}}_j$) all are plotted w.r.t z_j . Accretion disc parameters are $E = 1.001$, $L_0 = 2.906$, $\alpha = 0.01$. The disc and jet flow composition is described by $\xi = 1.0$ and relative mass outflow rate is $R_{\dot{m}} = 0.053$.

solid curve, the jet streamline is represented by dot-dashed curve, while the dotted curve shows the jet flow geometry. The arrows show the direction of the flow.

In Fig. (8a), we plot the combined accretion-jet solution, here the accretion Mach number M (solid) is plotted with respect to r , while the jet Mach number M_j is plotted w.r.t z_j in the same panel. In Figs. (8b-f), we plot various jet variables, for e.g. the jet three-velocity v_j (Fig. 8b), \mathcal{R}_j (Fig. 8c), Θ_j (Fig. 8d), Γ_j (Fig. 8e), and $\dot{\mathcal{M}}_j$ (Fig. 8f), for accretion disc parameters $E = 1.001$, $L_0 = 2.906$ and $\alpha = 0.01$. The jet is followed up to $z_j = 10^4 r_g$ above the equatorial plane of the accretion disc. In Schwarzschild metric we do not find multiple sonic points in jets, and jets are transonic flow also with only one sonic point. However, the jet achieves fairly high terminal speed ($\sim 0.11c$), inspite of being only thermally driven (i.e. v_j increases as Θ_j decreases). The specific energy of the jet \mathcal{R}_j and its entropy-accretion rate $\dot{\mathcal{M}}_j$ are constants of motion since the jet is assumed to be adiabatic.

We have shown in Figs. 2—4 that for given values of α , the nature of accretion solution depends on L_0 and since accretion disc launches the jet, we would like to analyse how the jet depends on the inner boundary condition of the flow. In Fig. (9a), we plot r_{sh} as a function of L_0 ; each curve is obtained for a given value of $E = 1.00001$ (solid, red), $E = 1.0001$ (dotted, blue) and 1.001 (dashed, black). The viscosity is given by $\alpha = 0.01$ and the disc-jet

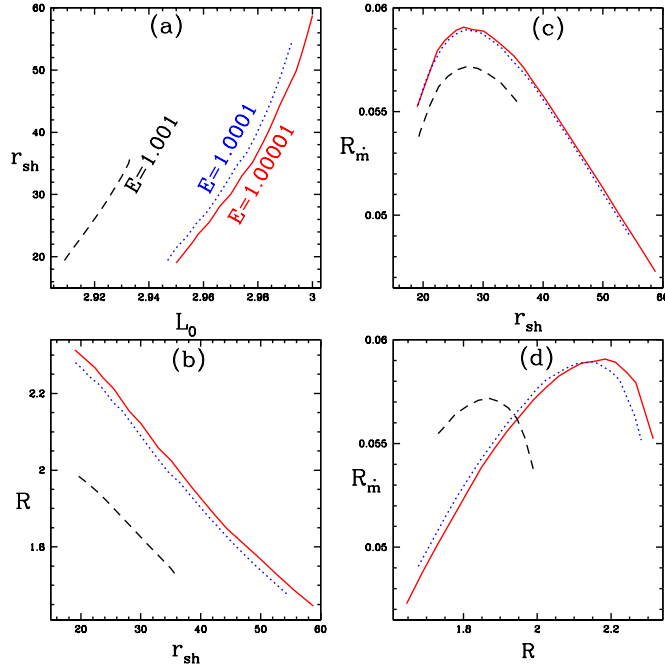


Figure 9. (a) Variation of shock location r_{sh} with L_0 ; (b) compression ratio R with r_{sh} ; (c) mass outflow rate $R_{\dot{m}}$ with r_{sh} and (d) $R_{\dot{m}}$ with R . Each curve is for $E = 1.00001$ (solid, red), 1.0001 (dotted, blue) and 1.001 (dashed, black). For all the cases, $\xi = 1.0$ and $\alpha = 0.01$.

is composed of electron-proton fluid. For a given value of L_0 , the r_{sh} increases with increasing E if steady shock is allowed by the flow, while for a given value of E , r_{sh} increases with L_0 . The corresponding compression ratio R as a function of r_{sh} is shown in Fig. (9b), while the relative mass outflow rates $R_{\dot{m}}$ (e.g. equation 49) are plotted with r_{sh} in Fig. (9c). As the r_{sh} increases, the compression ratio decreases (Fig. 9b) so the upward thrust becomes weaker. However, higher value of r_{sh} also makes the surface area of PSD and therefore the base of the jet larger, so the net mass flowing out as jet should become more. These contradictory tendencies cause the mass outflow rate to peak at some intermediate value of r_{sh} , as well as that of R (Fig. 9d).

In Figs. (10a-d), the converse dependence is studied where, r_{sh} is plotted with E , where each curve represent $L_0 = 2.95$ (solid, red), 2.94 (dotted, blue) and 2.93 (dashed, black). The composition of the flow and the viscosity parameter is the same as in Fig. (9a-d). The shock location increases (Fig. 10a) with both L_0 and E , as was observed in the previous figure. As the shock increases, the compression ratio decreases (Fig. 10b). However, $R_{\dot{m}}$ do not monotonically increase with decreasing r_s , for the same reason as was discussed in the previous figure. Interestingly, lower L_0 produces lower values of r_{sh} , but since these shocks are mainly rotation mediated, so lower L_0 implies weaker shock, and therefore the compression ratio R (\equiv the amount of squeezing on the post-shock flow) is weak too. Therefore, although

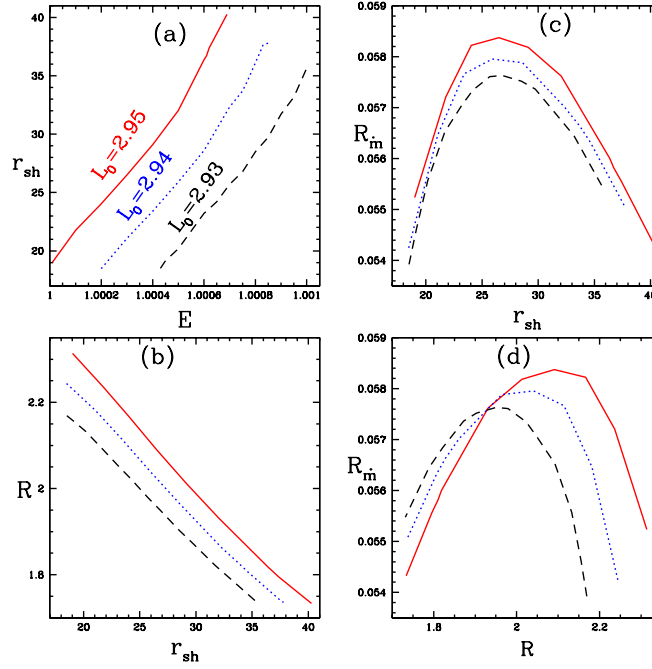


Figure 10. (a) Variation of r_{sh} with E , (b) R with r_{sh} , (c) \dot{M} with r_{sh} and (d) \dot{M} with R . Each curve is plotted for $L_0 = 2.95$ (solid, red), 2.94 (dotted, blue) and 2.93 (dashed, black). For all the curves, $\xi = 1.0$ and $\alpha = 0.01$.

the shock is located closer to the BH for lower L_0 , the \dot{M} is less even for the same values of r_{sh} .

4.2.1 Effect of viscosity, α

In Fig. (11a), we plot how r_{sh} would behave with the change in α , for fixed inner boundary condition or for the same values of E and L_0 . We plot the corresponding R as a function of r_{sh} (Fig. 11b) and \dot{M} with r_{sh} (Fig. 11c). Each curve is for constant $E = 1.0001$ (solid, red), $E = 1.00055$ (dotted, blue) and $E = 1.001$ (dashed, black), where for all curves $\xi = 1.0$, $L_0 = 2.94$. And in Fig. (11d), we plot R (solid, red), Σ (long dashed, magenta), Ξ (dotted, blue) and R_A (dashed, black) for $E = 1.0001$ (solid, red curve of Fig. 11a—c). Since E is a constant of motion for the accretion disc, and L_0 is the bulk angular momentum on the BH horizon, so fixed values of E and L_0 correspond to fixed inner boundary condition. For same L_0 and E , as one increases α , then the angular momentum at the outer edge of the disc would be higher. This implies that in the PSD too, the angular momentum L or specific angular momentum λ will be higher. Thus the shock location would increase with α . For a given E , the compression ratio decreases with increasing r_{sh} . Since the accretion shock is rotation dominated, therefore, the r_{sh} will increase for hotter flow (\equiv higher E), but the compression ratio will decrease. Thus, for a given value of α , \dot{M} will be less for higher

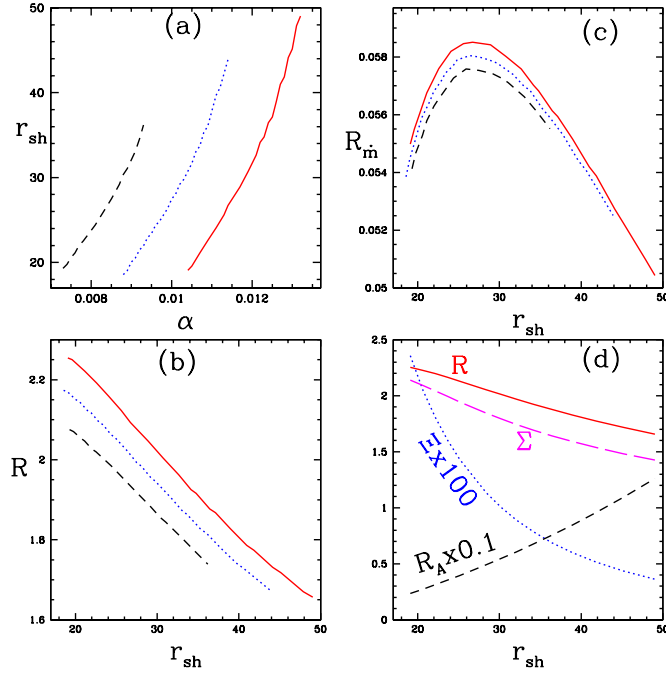


Figure 11. Variation of r_{sh} with α (a), R with r_{sh} (b), $R_{\dot{m}}$ with r_{sh} (c). Each curve is for $E = 1.0001$ (solid, red), $E = 1.00055$ (dotted, blue) and $E = 1.001$ (dashed, black). In panel (d), we plot R (solid, red), Σ (long dashed, magenta), Ξ (dotted, blue) R_A (dashed, black) for $E = 1.0001$ (solid, red curve of panels a–c). For all curves $\xi = 1.0$, $L_0 = 2.94$. Dependence of r_{sh} on α , for fixed inner boundary condition.

values of E . Fig. (11c) shows that the $R_{\dot{m}}$ is low for high and low values of r_{sh} and maximizes at some intermediate value. In Fig. (11d), we find out why the mass outflow rate or $R_{\dot{m}}$ has a non-uniform dependence on r_{sh} . From equation (52), we know that $R_{\dot{m}}$ increases with increasing R_A , R and Ξ , but decreases with increasing Σ . So as the r_{sh} increases (Fig. 11a), Fig. (11d) shows that R and Ξ decrease, which implies that the post-shock thrust which is responsible for driving the jet decreases which should decrease $R_{\dot{m}}$. However, R_A , or the ratio between jet cross-sectional area and the PSD surface area, increases; therefore, this should increase $R_{\dot{m}}$. These two contradictory tendencies, make $R_{\dot{m}}$ attain low values when the r_{sh} is very close to horizon and when it is far away, but maximize for some intermediate values.

Let us compare the flow variables of accreting matter which starts with the same outer boundary condition. We plot and compare the three velocity v (Fig. 12a), sound speed a (Fig. 12b) and the bulk angular momentum L (Fig. 12c) of accretion flows starting with the same outer boundary condition $E = 1.0001$ and $\lambda_{\text{out}} = \lambda_K = 140.85$ at the outer edge of the accretion disc $r_{\text{out}} = 19835.3$. Each curve represents the solution for $\alpha = 0.01$ (solid, red), $\alpha = 0.0105$ (dotted, blue) and $\alpha = 0.011$ (dashed, black), and the net relative mass outflow computed were $R_{\dot{m}} = 0.047$ (solid, red), $R_{\dot{m}} = 0.059$ (dotted, blue) and $R_{\dot{m}} = 0.054$

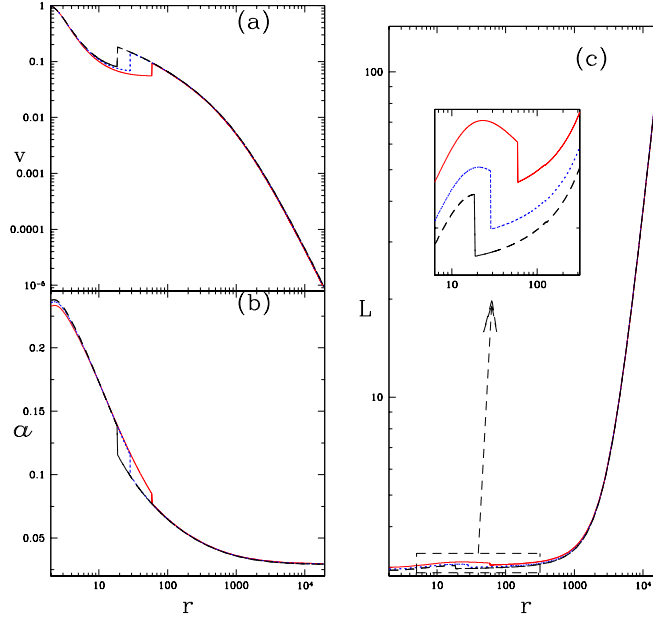


Figure 12. Three-velocity v (a), local sound speed a (b) and bulk angular momentum L (c) of the accretion disc plotted with r . Each curve is for $\alpha = 0.01$ (solid, red), $\alpha = 0.0105$ (dotted, blue) and $\alpha = 0.011$ (dashed, black). For all the curves, the outer boundary is at $r_{\text{out}} = 19835.3r_g$, the corresponding specific angular-momentum is the Keplerian angular momentum at r_{out} , i.e. $\lambda_{\text{out}} = \lambda_K = 140.85$ and the constant of motion for all the curves is $E = 1.0001$. Inset in panel (c) zooms on the L distribution around the location of the shock.

(dashed, black). As α is increased, the net angular momentum of the inner disc decreases, and since the shock is rotation driven, lower angular momentum causes r_{sh} to decrease (see the inset of Fig. 12c).

Although it is interesting to show how α will affect r_{sh} , for the same inner boundary condition of the disc. But the physics of accretion disc is controlled by outer boundary condition, so it will be more physical to study how the disc solution, as well as, the ensuing jet solutions depend on α when the outer boundary condition of the accretion disc is kept the same. In Fig. (13a), r_{sh} is plotted with α for $E = 1.0001$. The outer boundary of the disc is $r_{\text{out}} = 16809.016$ for all solutions for which the curve is plotted. The specific angular momentum at r_{out} is the local Keplerian value $\lambda_{\text{out}} = \lambda_K = 129.662$. Since E is a constant of motion for all the solutions presented, and λ_{out} is also same for all the disc solutions, so comparing solutions for same E and λ_{out} is equivalent to comparing solutions starting with the same outer boundary. Viscosity transports angular momentum outwards; therefore, for a given value of E , the shock moves closer to the BH as viscosity is increased. So r_{sh} decreases with increasing α . The corresponding dependence of R (solid, red), Ξ (dotted, blue), Σ (long dashed, magenta) and R_A (dashed, black) with α has been plotted in Fig. 13b. The shock becomes stronger as it moves towards the horizon therefore R increases, but the enhanced

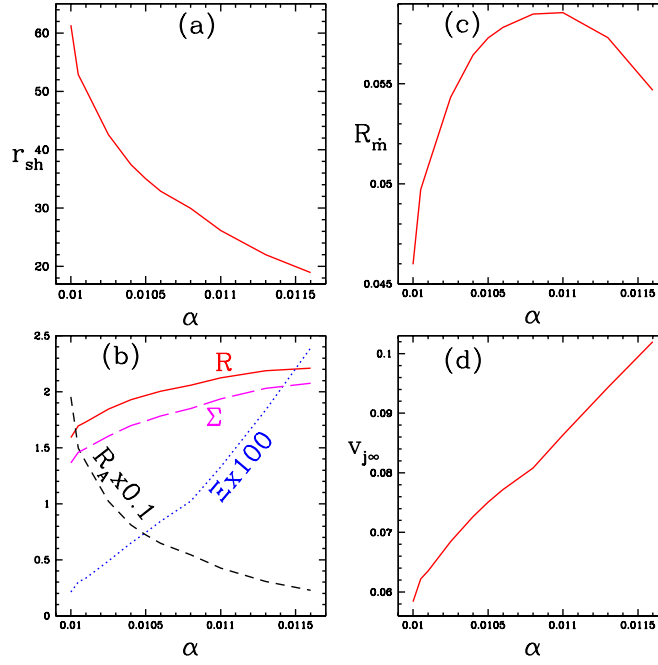


Figure 13. (a) Variation of r_{sh} with α , (b) R (solid, red), Ξ (dotted, blue), Σ (long dashed, magenta) and R_A (dashed, black) with α , (c) R_m with α and (d) $v_{j\infty}$ with α . The outer boundary is at $r_{\text{out}} = 16809.016$, and corresponding specific angular momentum is the Keplerian angular momentum at r_{out} , i.e. $\lambda_{\text{out}} = \lambda_K = 129.662$. For all the curves, $E = 1.0001$, $\xi = 1.0$. Dependence of r_{sh} on α for fixed outer boundary.

compression also squeezes more matter along the jet channel so Ξ increases too. However, Σ increases and R_A decreases which should decrease the R_m . Such antagonistic tendencies make the R_m to peak at some intermediate α , as is depicted in Fig. (13c). In Fig. 13d, the jet terminal speed $v_{j\infty}$ with α is plotted. Since R increases, so the upward thrust also increases, making jets stronger, even if R_m decrease. It means we can have stronger but lighter jets.

4.2.2 Effect of composition, ξ

In all the previous figures, we dealt with fluid composed of only electrons and protons. Chattopadhyay & Ryu (2009) showed that if the proton proportion is reduced (where the charge balance is maintained by proportionate increase of positrons), the flow becomes thermally more relativistic because the decrease in thermal energy is compensated by decrease in inertia of the flow. Fig. (14a) shows that r_{sh} increases with ξ , where each curve is for $E = 1.0001$ (solid, red), 1.00055 (dotted, blue) and 1.001 (dashed, black), and $L_0 = 3.0$ and $\alpha = 0.01$. Higher r_{sh} implies lower R (Fig. 14b); as a result, R_m decrease with increasing r_{sh} , although, due to the related increase in the jet base and other factors [dealt with related to Figs. 11(a)-(d)], R_m peaks at some intermediate value (Fig. 14c). In Fig. (14d), the terminal speed of the jet $v_{j\infty}$ with r_{sh} is plotted. As the shock recedes, the speed of the jet decreases,

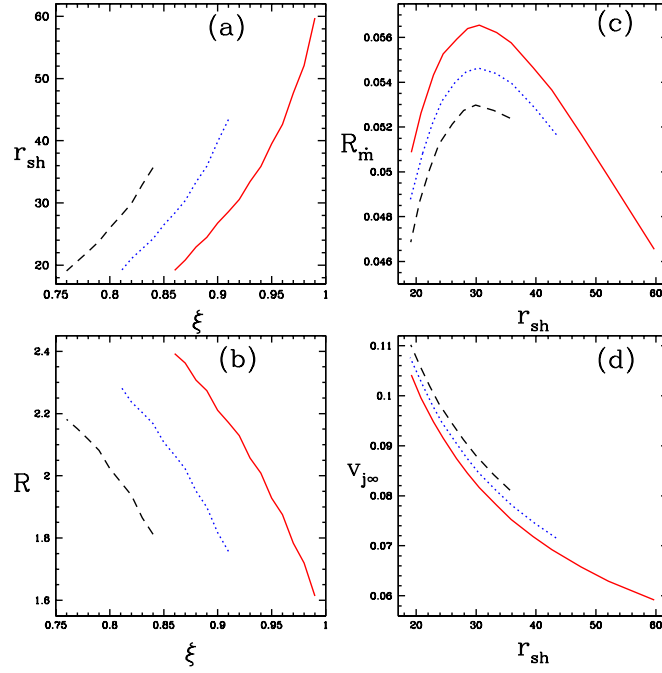


Figure 14. Dependence of r_{sh} on composition parameter ξ (a), R with ξ (b), $R_{\dot{m}}$ on r_{sh} (c) and $v_{j\infty}$ with r_{sh} (d). Each plot corresponds to $E = 1.0001$ (solid, red), 1.00055 (dotted, blue) and 1.001 (dashed, black). For all the curves $L_0 = 3.0$, $\alpha = 0.01$.

even where $R_{\dot{m}}$ is increasing. But if the accretion disc flow is more energetic, the jet terminal speed is higher, although $R_{\dot{m}}$ is lower.

In Figs. 15(a) and b), we plot the shock parameter space in the $E - L_0$ space for various combinations of viscosity and composition parameters like $\xi, \alpha = 1.0, 0.01$ (solid), 1.0, 0.02 (dotted), 0.27, 0.01 (dashed) and 0.27, 0.02 (long dashed) in Fig. 15(a) and for $(\xi, \alpha) = 0.25, 0.01$ (solid), 0.25, 0.02 (dotted) and 0.0625, 0.01 (dashed) in Fig. 15(b). The shaded region indicates the steady shock region of the parameter space when mass-loss is considered. Similar to the inviscid study (Chattopadhyay & Chakrabarti 2011), the shock parameter space moves to the higher energy direction of the parameter space till ξ is reduced from 1 to 0.27. As ξ is reduced further, the shock parameter space moves towards the low-energy side. The reduction of steady shock parameter space due to mass-loss actually indicates that shock in accretion actually exists in a wide range, but only as a time-dependent one.

5 DISCUSSIONS AND CONCLUSIONS

Investigations of viscous accretion disc around a BH in general relativistic regime are important, because a BH is necessarily a relativistic object, and close to the horizon the departure from Newtonian description is significant. Analysis with Paczyński-Wiita pNp gives us an overall qualitative understanding, but quantitatively the results or predictions based on pNp

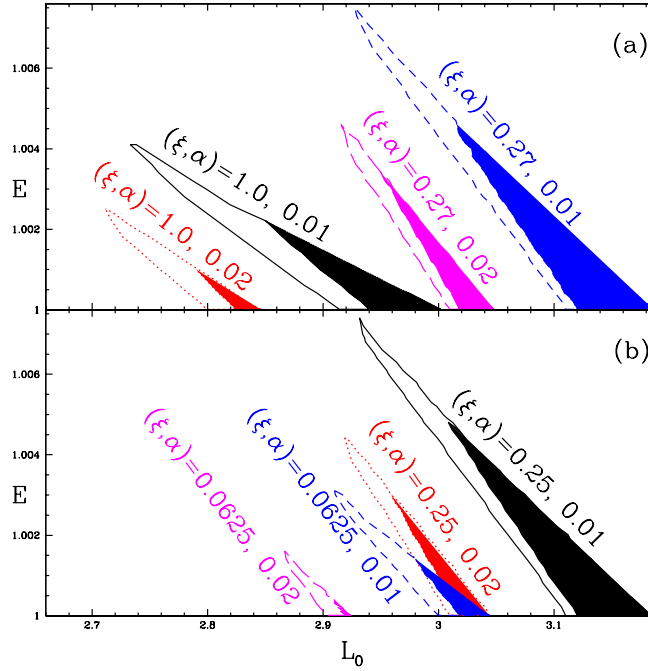


Figure 15. (a) Comparison of the shock parameter space in $E - L_0$ with mass-loss (shaded area) and without mass-loss (bounded area) for different disc parameters, $\xi, \alpha = 1.0, 0.01$ (solid), $1.0, 0.02$ (dotted), $0.27, 0.01$ (dashed) and $0.27, 0.02$ (long dashed). (b) Comparison of shock parameter space $E - L_0$ for $(\xi, \alpha) = 0.25, 0.01$ (solid), $0.25, 0.02$ (dotted) and $0.0625, 0.01$ (dashed). Same notations for shocked region with or without mass-loss.

are bound to be wrong. One of the artefacts of pNp is that the disc closer to the horizon is hotter than they actually are. Moreover, matter speed exceeds the speed of light. Furthermore, the relativistic shear tensor is more complicated than the Newtonian variant. All these reasons influenced us to re-investigate the self-consistent, simultaneous, viscous accretion-ejection solutions around BHs in the general relativistic regime. We chose the simplest type of BH for our study, simply because the influence of Kerr metric in powering jets is not very conclusive in some of the studies made on microquasars (Fender et al. 2010).

In this paper, we first analysed only the accretion solution (i.e. assuming $R_{in} = 0$). The solution procedure was influenced by the methodology laid down by Becker and his collaborators in the pNp regime in order to find the sonic points self-consistently. We have generalized it for general relativistic domain. Moreover, the equation of the state of flow is also relativistic and not a Newtonian polytropic gas, as was used by Becker. We obtained all possible accretion solutions in the advective domain, starting from Bondi type (single r_{co} -type sonic point), solutions where multiple sonic points formed, shocked solution and ADAF solutions (single r_{ci} -type sonic points). All of these various solutions were obtained for various combinations of E , L_0 and α , so in this respect each solution is a three-parameter class of solutions. A quick comparison shows that, in the pNp regime shocks are stable for

higher viscosity parameters ($\alpha \sim 0.3$), but in the general relativistic regime (solutions of this paper) shock remains steady for much lower values ($\alpha \lesssim 0.06$). In the pNp regime, the shear tensor is much simpler, and the $r - \phi$ component is proportional to the radial derivative of the angular velocity (Kumar & Chattopadhyay 2013), but in the GR regime the shear tensor is much more complicated and depends on four-velocities and their derivatives, as well as various components of four-acceleration. The approximated version used in this paper also has radial four-velocity term in addition to the derivative of azimuthal component of four-velocity (see equation 9). As a result, the shock is made unstable for lower values of α . Instability of shock is actually good because not only such oscillation explains quasi-preiodic oscillations (QPOs) but also does additional pumping to generate stronger jet (Das *et al.* 2014).

In this paper, we did a detailed study of jet morphology based on the works of Chakrabarti (1985, and citations therein). Here too, physics in curved space-time differed from Newtonian or pNp regime. In GR, the entropy constant surface in non-equatorial plane for adiabatic flow coincides with constant angular momentum surfaces called VZS which are not cylinders of flat space-time. Chakrabarti (1985) showed ways to relate these surfaces with angular momentum of the flow. Since jets are tenuous and are likely to be adiabatic till they interact with the ambient medium, so adiabatic jet is a fairly good assumption. Therefore, VZS becomes the natural streamline of the flow. Interestingly, the accreting matter has predominantly the radial and azimuthal component of four-velocity, and can be quite accurately described about the equatorial plane; however, the jet has all three components of the four-velocity. We turned this essentially three spatial dimensional problem into an effective one-dimensional problem, by projecting jet equations of motion along the streamline defined by VZS and the methodology is properly defined in Section 2.3 and Appendix A. The streamline obtained in such a manner is very rich, where some combination of parameters produced partially pinched-off streamlines, which are ripe case for multiple sonic points and internal shocks in jets. However, in Schwarzschild geometry above the equatorial plane, such jet geometry cannot be connected to the inner disc region of the accreting matter. Only those VZS solutions which did not allow multiple sonic points were found to be relevant, and therefore we only obtained monotonic jet solutions. So depending on where the shock in accretion disc forms, the jet base and jet flow geometry change. This fact is also markedly different from pNp prescription, since in pNp prescription the jet geometry is weakly dependent on the jet base or other accretion disc properties.

The response of the shock location with viscosity is similar to our studies in pNp. Even relativistic viscosity makes the accretion shock to move closer to the event horizon as it is increased, if the outer boundary condition of the accretion disc is kept the same. As the shock moves closer to the BH, compression ratio across the shock increases, which generally increases the jet strength. This initially increases the relative mass outflow rate, but the mass outflow rate starts to drop, as the shock moves closer to the BH. We also showed that as the shock becomes stronger (forms closer to the BH), it also increases the upward thrust (Figs. 11d, 13b). Independent of how much percentage of accreting matter is pumped out as jets, because of the increased thrust the terminal speed of the jet material increases with decreasing shock location. The shock cannot move too close to the BH and still remain stationary, at some point it will become unstable and start to oscillate. And that is marked by the closest limit up to which we found steady shocks in this analysis. Although this investigation is steady state and cannot conclusively comment on essentially time-dependent phenomena, but it can be conjectured that increasing viscosity even more should increase the oscillation frequency of the shock too. Such a situation does mimic an outbursting source, where it had been shown that as the object moves from low hard state to intermediate states, the QPO as well as the jet strength increases. We also showed that fluid described by a proton proportion of 27% of the electron number density (the rest being positrons), or $\xi = 0.27$ is thermally the most relativistic, and can form shocks in accretion in the largest portion of the $E - L_0$ parameter space. We also showed that shock in accretion does not form if the accretion disc is composed of pair plasma. And the mass outflow rate is less than 6% of the accretion rate for any value of ξ . We also showed that independent of the composition of the flow, hotter the accretion disc, faster will be the emanating jet, although the mass outflow rate may not be very high.

ACKNOWLEDGEMENTS

The authors acknowledge the anonymous referee for fruitful suggestions to improve the quality of the paper.

REFERENCES

- Aktar R., Das S., Nandi A., 2015, MNRAS, 453, 3414
 Becker P. A., Das S., Le T., 2008, ApJ, 677, L93

- Blumenthal G. R., Mathews W. G. 1976, ApJ, 203, 714.
- Bondi H.; 1952, MNRAS, 112, 195
- Chakrabarti S. K., 1985, ApJ, 288, 7
- Chakrabarti S.K., 1989, ApJ, 347, 365
- Chakrabarti S.K., 1996, ApJ, 464, 664
- Chandrasekhar S., 1939, An Introduction to the Study of Stellar Structure. Univ. Chicago Press, Chicago, IL
- Chattopadhyay I., 2008, in Chakrabarti S. K., Majumdar A. S., eds, AIP Conf. Ser. Vol. 1053, Proc. 2nd Kolkata Conf. on Observational Evidence of Black Holes in the Universe and the Satellite Meeting on Black Holes Neutron Stars and Gamma-Ray Bursts. Am. Inst. Phys., New York, p. 353
- Chattopadhyay I., Chakrabarti S.K., 2011, Int. J. Mod. Phys. D, 20, 1597
- Chattopadhyay I., Das S., 2007, New Astron., 12, 454
- Chattopadhyay I., Kumar R., 2013, in Das S., Nandi A., Chattopadhyay I., eds, Astronomical Society of India Conference Series, Vol. 8, p. 19
- Chattopadhyay I., Ryu D., 2009, ApJ, 694, 492
- Cox J. P., Giuli R. T., 1968, Principles of Stellar Structure, Vol.2: Applications to Stars. Gordon and Breach, New York
- Das S., 2007, MNRAS, 376, 1659
- Das S.; Chattopadhyay I., 2008, New Astron., 13, 549.
- Das S., Chattopadhyay I., Nandi A., Molteni D., 2014, MNRAS, 442, 251.
- Doeleman S. S. et al., 2012, Science, 338, 355.
- Fender R. P., Gallo E., 2014, Space Sci. Rev., 183, 323
- Fender R. P., Belloni T. M., Gallo E., 2004, MNRAS, 355, 1105
- Fender R. P., Gallo E., Russell D., 2010, MNRAS, 406, 1425
- Fukue J., 1987, PASJ, 39, 309
- Gallo E., Fender R. P., Pooley G. G., 2003, MNRAS, 344, 60
- Giri K., Chakrabarti S. K., 2013, MNRAS, 430, 2826
- Gu W.-M., Lu, J.-F., 2004, Chin. Phys. Lett., 21, 2551
- Junor W., Biretta J. A., Livio M., 1999, Nature, 401, 891
- Kozłowski, M., Jaroszynski, M., Abramowicz, M. A., 1978, A&A, 63, 209
- Kumar R., Chattopadhyay I., 2013, MNRAS, 430, 386
- Kumar R., Chattopadhyay I., 2014, MNRAS, 443, 3444

- Kumar R., Singh C. B., Chattopadhyay I., Chakrabarti S. K., 2013, MNRAS, 436, 2864
- Kumar R., Chattopadhyay I., Mandal S., 2014, MNRAS, 437, 2992
- Lanzafame G., Molteni D., Chakrabarti S. K., 1998, MNRAS, 299, 799
- Lasota J. P., 1994, in Duschl W. J., Frank J., Meyer F., Meyer-Hofmeister E., and Tscharnutter W. M., eds, Theory of Accretion Disks 2. Kluwer, Dordrecht, p. 341
- Lee, S.-J., Ryu D., Chattopadhyay I., 2011, ApJ, 728, 142
- Liang E. P. T., Thompson K. A., 1980, ApJ, 240, 271
- Lu J. F., 1985, A&A, 148, 176
- Lu J. F., Gu W. M., Yuan F., 1999, ApJ, 523, 340
- McHardy I. M., Koerding E., Knigge C., Fender R. P., 2006, Nature, 444, 730
- Molteni D., Lanzafame G., Chakrabarti S. K., 1994, ApJ, 425, 161
- Molteni D., Sponholz H., Chakrabarti S. K., 1996a, ApJ, 457, 805
- Molteni D., Ryu D., Chakrabarti S. K., 1996b, ApJ, 470, 460
- Narayan R., Kato S., Honma F., 1997, ApJ, 476, 49
- Novikov I. D.; Thorne K. S., 1973, in Dewitt B. S., Dewitt C., eds, Black Holes. Gordon and Breach, New York, p. 343
- Paczynski B. and Wiita P. J., 1980, A&A, 88, 23.
- Peitz J., Appl S., 1997, MNRAS, 286, 681
- Riffert H., Herold H., 1995, ApJ, 450, 508
- Ryu D., Chattopadhyay I., Choi E., 2006, ApJS, 166, 410
- Shakura N. I., Sunyaev R. A., 1973, A&A, 24, 337S.
- Sunyaev R. A.; Titarchuk L. G.; 1980, A&A, 86, 121
- Synge J. L., 1957, The Relativistic Gas, North-Holland Publishing Co., Amsterdam
- Takahashi R., 2007, MNRAS, 382, 567
- Taub A. H., 1948, Phys. Rev., 74, 328
- Vyas M. K., Kumar R., Mandal S., Chattopadhyay I., 2015, MNRAS, 453, 2992

APPENDIX A: CALCULATION OF h_p^2

The equation of tangent is defined on jet streamline at any point,

$$x_p = mr_j \sin \theta_j + c_i, \quad (\text{A1})$$

where $m = \frac{dy}{dx} = (r_j - 2)\cot\theta_j + (r_j - 3)\tan\theta_j$ and c_i are the slope and intercept of the tangent, respectively. The basis vector along jet streamline is defined as,

$$\mathbf{e}_p = \left(\frac{\partial r_j}{\partial x_p}\right)\mathbf{e}_r + \left(\frac{\partial \theta_j}{\partial x_p}\right)\mathbf{e}_\theta, \quad (\text{A2})$$

where, $\mathbf{e}_p = h_p \hat{e}_p$, $\mathbf{e}_r = h_r \hat{e}_r$ and $\mathbf{e}_\theta = h_\theta \hat{e}_\theta$. Here, \hat{e}_p , \hat{e}_r and \hat{e}_θ are unit basis vectors along tangent, radial and polar direction, respectively. The magnitude of this basis vector is defined as,

$$h_p^2 = h_r^2 \left(\frac{\partial r_j}{\partial x_p}\right)^2 + h_\theta^2 \left(\frac{\partial \theta_j}{\partial x_p}\right)^2, \quad (\text{A3})$$

where $h_r^2 = g_{rr} = (1 - 2/r_j)^{-1}$ and $h_\theta^2 = g_{\theta\theta} = r_j^2$ are metric components. In order to obtain h_p , we have to take partial differentiation with respect to x_p of equations (37) and (A1), we get

$$\begin{aligned} \left[\frac{(r_j - 3)}{r_j(r_j - 2)}\right]^2 \left(\frac{\partial r_j}{\partial x_p}\right)^2 &= \cot^2\theta_j \left(\frac{\partial \theta_j}{\partial x_p}\right)^2 \quad \text{and} \\ \cos^2\theta_j &= [2r_j - 2 - \sin^2\theta_j]^2 \left(\frac{\partial r_j}{\partial x_p}\right)^2 + r_j^2 \tan^2\theta_j [r_j - 4 + \sin^2\theta_j]^2 \left(\frac{\partial \theta_j}{\partial x_p}\right)^2. \end{aligned} \quad (\text{A4})$$

Now, expression of h_p is obtained by using equation (A4) in equation (A3),

$$h_p^2 = \left(1 - \frac{2}{r_j}\right)^{-1} \left[\frac{\cos^2\theta_j + \sin^2\theta_j(r_j - 3)^2/(r_j(r_j - 2))}{\{2r_j - 2 - \sin^2\theta_j\}^2 + \{\tan^2\theta_j(r_j - 4 + \sin^2\theta_j)(r_j - 3)/(r_j - 2)\}^2} \right] \quad (\text{A5})$$